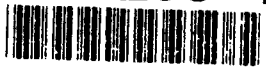

Sponsored by

DEFENSE ADVANCED RESEARCH PROJECTS AGENCY

OPTOELECTRONICS MATERIAL CENTER

A Collaborative Program including:

Center for High Technology Materials
of the University of New Mexico,
Stanford University, and
California Institute of Technology

ARPA Order No. 7526
Issued by DARPA/CMO under Contract #MDA972-90-C-0046

REPORT DOCUMENTATION PAGE

Form Approved
OMB No. 0704-0188

1. AGENCY USE ONLY (Leave blank)	2. REPORT DATE	3. REPORT TYPE AND DATES COVERED
	15 May 1992	Quarterly 1 Jan 91 - 31 Mar 91

4. TITLE AND SUBTITLE
Optoelectronic Materials Center, a Collaborative Program including University of New Mexico, Stanford University, and California Institute of Technology

5. FUNDING NUMBERS
MDA972-90-C-0046

6. AUTHOR(S)
S.R.J. Brueck, Editor

7. PERFORMING ORGANIZATION NAME(S) AND ADDRESS(ES)
University of New Mexico
Center for High Technology Materials
EECE Building, Room 125
Albuquerque, NM 87131-6081

8. PERFORMING ORGANIZATION REPORT NUMBER

9. SPONSORING/MONITORING AGENCY NAME(S) AND ADDRESS(ES)
Defense Advanced Research Projects Agency
ARPA Order No. 7526 Issued by DARPA/[illegible] TO
under Contract #MDA972-90-C-0046

10. SPONSORING/MONITORING AGENCY REPORT NUMBER

11. SUPPLEMENTARY NOTES

12a. DISTRIBUTION AVAILABILITY STATEMENT

12b. DISTRIBUTION CODE

13. ABSTRACT (Maximum 200 words)

The Optoelectronic Materials Center is a collaborative program involving the University of New Mexico, Stanford University, and the California Institute of Technology. Sandia National Labs and MIT Lincoln Lab are also involved in this program under separate contract vehicles. This orogram emphasizes three main areas:

diode-based visible sources
two-dimensional optical interconnects
high-speed optoelectronics

Progress on individual tasks is very briefly discussed below. Several of the tasks will impact more than one of the above areas. For simplicity, the tasks are arranged by institution in an order roughly determined by the above areas.

14. SUBJECT TERMS
Diode-based visible sources, two dimensional optical interconnects, high-speed optoelectronics

15. NUMBER OF PAGES
53 including cover

16. PRICE CODE

17. SECURITY CLASSIFICATION OF REPORT	18. SECURITY CLASSIFICATION OF THIS PAGE	19. SECURITY CLASSIFICATION OF ABSTRACT	20. LIMITATION OF ABSTRACT
unclassified	unclassified	unclassified	unclassified

DARPA QUARTERLY STATUS REPORT

January - March 1991

UNIVERSITY OF NEW MEXICO

Visible Diode Lasers

We have fabricated visible laser diodes in AlGaAs/strained AlGaInAs MOCVD materials lasing at 675 nm with output powers up to 600 mW using 1 msec pulses. Thresholds are several kA/cm^2 but the strained QWs appear to improve the reliability. Unstrained wells for the same structure did not lase at up to kA/cm^2 pump current. Further tests and characterization are planned.

Epitaxial structures have been grown for second harmonic generation in GaAs and green light observed in these structures. Extensive experiments aimed at growth of HBT and p-n-p-n optical switches have been undertaken. with results showing good performance using carbon doping of the base layer. These devices have been monolithically integrated with VCSEL diodes to form the first optical logic elements of this type. This technology utilizes the results of our regrowth experiments and multi-step MOCVD epitaxy. Please refer to the report on device results for details.

Facility engineering and architechtural designs are nearly completed for the Crystal Growth Facility Expansion project (Joint with NMRDI). Preliminary design work has been completed on the new MOCVD reactor, and Dr. Schaus traveled to Europe to evaluate custom MOCVD equipment vendors. Building bid requests should be distributed on July 17th. The MOCVD reactor bid request should go out in late July as well. *(C. F. Schaus)*

Vertical Cavity Surface-Emitting Lasers

A new epitaxial structure for a vertical-cavity surface-emitting laser (VCSEL) was designed and grown by MOCVD. It consists of a multiquantum well, graded-index, separate-confinement-hetero-structure (GRINSCH) active layer bounded by quarter-wave, multilayer reflectors (MLR) with graded interfaces. Using a planar device design with proton-implanted current-confinement, we have fabricated VCSELs with record cw performance characteristics at room temperature, including the lowest series resistance (20 Ω), threshold voltage (2.4 V), current density (740 A/cm^2) ever reported. In addition, these VCSELs have demonstrated high differential quantum efficiency (80%), high power conversion efficiency (6%), low threshold current (2 mA), and high optical output power (2 mW), which are comparable to or better than those of state-of-the-art devices grown by MBE. These improved characteristics were achieved largely by the continuous grading of the hetero-interfaces in the reflectors, which reduced the energy barriers that impede carrier transport and eliminated a significant contribution to the series resistance. These VCSELs comfortably meet all of the performance goals set forth in our DARPA milestones. (Cheng, Schaus, and Sun)

Spatial Light Modulator Arrays

A mask set for arrays of multi-quantum-well spatial light modulators has been designed, including arrays of symmetric SEEDS. A reflection-mode GaAlAs/GaAs SEED epitaxial structure has also been grown. Device fabrication and testing are in progress. (Cheng)

High-power Picosecond Pulse Generation Using Diode Lasers for Widespread Optical Clock Distribution and Time-division Multiplexing

Three high-power external cavity laser experiments have been designed and constructed:

1. static mode filtering of wide stripe lasers using unstable resonator geometry,
2. active mode-locking of wide stripe laser,
3. additive (coupled-cavity) mode-locking experiment.

Experiment 1 has achieved single transverse mode operation up to 250 mW and single longitudinal mode operation with narrow linewidth (instrument-limited at 0.05 nm) up to 550 mW, with 100 and 150 μm stripe lasers driven by 10 to 100 ns pulses at 10 kHz repetition rate. The lasers had their internal facets anti-reflection (AR) coated (residual reflectivity < 1%) for good external cavity coupling efficiency.

Experiment 2 has demonstrated 50 ps pulses with extensive sub-structure and poor spectral characteristics due to imperfect AR coatings. One laser diode with good AR coatings gave good results but its lifetime was short (~ 10 h).

Experiment 3 is still under construction, and is expected to begin on July 1.

The following problems have surfaced:

1. poor reliability of first batch of wide-stripe laser diodes (fabricated in-house). A second batch is being prepared.

2. lack of reproducibility and occasional device damage in e-beam dielectric evaporator during AR coating process. Time has been reserved on a magnetron sputtering setup (a system used for research by another professor in the department) which should yield more reproducible results. (J.G. McInerney)

Visualization of Complex 3D Integrated Circuits

Infrared sources

We have studied a technique to generate long (more than 100 pulses of approximately 10 ps duration, at 1.06 μm. The technique is called Passive Negative Feedback, and has been the object of a detailed review paper, to be completed in the next reporting period. Unfortunately, the goal of stable extended train of pulses of less than 10-ps duration has not been reached yet with the arc lamp pumped Nd:YAG source, because of problems associated with thermal lensing in the two rod cavity required for this operation, as well as thermal birefringence.

This source is designed for switching small electrical circuits (coplanar striplines), and probing the electric field.

Copper Vapor Laser Pumped Amplifier

The plasma tube of the Metallasor technology copper vapor laser to pump the femtosecond amplifier (used for imaging) failed and had to be replaced. Shortly thereafter, the thyratron failed and had to be replaced.

Imaging

Despite the repeated breakdown of the copper vapor laser, we have been able to demonstrate the imaging using visible radiation, an image intensifier, and a reticon detector as two-dimensional detector. Depth resolution is achieved by type II up-conversion in a urea crystal. A publication has been submitted to Applied Optics on this phase of the work. (J.-C. Diels)

Thermal Properties of Electrically Pumped VCSELs

In spite of severity of thermal problems in vertical-cavity surface emitting lasers, there has been no adequate treatment of thermal properties of these devices. Previous approaches suffered from oversimplified assumptions such as one-dimensional heat flow or absence of Joule heating. We have developed a comprehensive two-dimensional thermal-electrical self-consistent model of etched-well double-heterostructure VCSELs. Major heat sources have been identified and their spatial distribution has been determined by analyzing current spreading in the device. Temperature profiles due to individual heat sources have been calculated and their aggregate effect has been examined. Various new aspects of etched-well VC-SEL behavior have been revealed. Unless careful design is undertaken, the device may suffer from poor overlap between the optical field and gain profiles, which inevitably would increase its threshold. Novel horizons for thermal waveguide engineering are opened by ability to control the sign and magnitude of the guiding effect simply by changing the N-$Al_{0.3}Ga_{0.7}As$ layer doping. Thermal behavior can be improved significantly by increasing the P-$Al_{0.3}Ga_{0.7}As$ layer doping.

Milestones for the next quarter include: 1) Optimization of the design of etched-well VCSELs aimed at maximizing the output power; 2) Thermal analysis of two-dimensional arrays of etched-well VCSELs. (Marek Osinski)

The following papers have been submitted:

M. Osinski, *Vertical-cavity surface-emitting semiconductor lasers: Present status and future prospects* (invited paper), SPIE Symposium on High Power Lasers, OE/LASE'91, Los Angeles, California, January 20-25, 1991.

W. Nakwaski and M. Osinski, *Thermal properties of etched-well surface-emitting semiconductor lasers*, IEEE Journal of Quantum Electronics.

W. Nakwaski and M. Osinski, *Temperature profiles in etched-well surface-emitting semiconductor lasers*, Japanese Journal of Applied Physics (Letters).

W. Nakwaski and M. Osinski, *Thermal waveguiding in etched-well surface-emitting diode lasers*, CLEO '91 Conference on Lasers and Electro-Optics, Baltimore, Maryland, May 12-17, 1991.

Optically Pumped DFB-RPG VCSELs

A novel distributed-feedback resonant-periodic-gain structure for vertical-cavity surface-emitting lasers has been proposed and demonstrated. Compared to recently developed DBR-RPG structures, a reduction in the total thickness of the device by almost a factor of two is achieved by eliminating the end reflectors and by interlacing the quarter-wave multilayer high reflectors with the RPG medium. The DFB-RPG devices offer the advantages of considerably simpler fabrication process, improved wavelength selectivity, and strong discrimination against excitation of secondary longitudinal modes. Room-temperature cw and pulsed operation has been achieved using a prototype device grown by MOCVD at CHTM Crystal Growth Facility. Preliminary data obtained on optically pumped bare wafer sample without any heat sink indicate

that very high output power should be possible. 6.7 mW cw and 8.5 W pulsed output power was measured.

The milestone for the next quarter is to explore high-output power limits under pulsed conditions. (M. Osinski)

Paper submitted:

M. Mahbobzadeh and M. Osinski, *Novel distributed-feedback structure for surface-emitting semiconductor lasers*, SPIE Symposium on High Power Lasers, OE/LASE'91, Los Angeles, California, January 20-25, 1991.

STANFORD UNIVERSITY

The Stanford projects are directed in two major directions: 1) the development of visible light sources, and 2) development of high speed optical modulators and detectors for optical interconnects, processing and computing. Progress for the period 1/1/91 through 3/3/91 is reported below.

Visible Light Sources

Second Harmonic Generation in Periodically-Poled Materials

The goal of this program is to demonstrate efficient generation of visible radiation by quasi-phase-matched second harmonic generation (SHG) in periodically-poled ferroelectric waveguides. Prior to the start date of the DARPA program, we demonstrated lithographically defined periodic domain inversions in lithium niobate, subsequent waveguide fabrication by annealed proton exchange, and generation of green and blue light by SHG in the waveguides. Our goal for the first year of the DARPA program is to improve the efficiency of these devices to the point where it is possible to generate > 1mW of blue light.

Our initial focus has been on improving our understanding of the annealed proton exchange (APE) process, as it appears to be limiting the efficiency of the device both through axial inhomogeneities, which spoil the phase matching by inducing axial variations in the phase velocity, and through a reduction of the nonlinear susceptibility dependent on the proton dose. Characterization of APE is complicated by the nonlinear diffusion coefficient, and the nonlinear dependence of the index of refraction on the proton concentration. We have developed a model for the nonlinear diffusion and the dispersion, based on measurements of wavelength dependent modal effective indices and modal intensity profiles, that appears to adequately describe the evolution of the concentration profile with annealing over all practical concentration regimes and the optical properties from 400 nm - 1300 nm. This model will be used to design improved waveguides for more efficient devices, and is being prepared for publication. (Fejer)

Development of II-VI Materials

Work has progressed in two areas related to materials growth for nonlinear frequency conversion: 1) fabrication of laterally patterned II-VI layers for quasi-phase matching (QPM) and 2) growth of ZnSe on GaAs. In the first quarter, we reported growth of alternating polycrystalline and <111>CdTe stripes on <100>GaAs substrates, which were patterned with silicon dioxide stripes. The second harmonic intensity observed from the CdTe over the silicon dioxide is lower than that of the CdTe grown on bare GaAs. This result suggests that lateral modulation of the nonlinear coefficient is possible using this structure. However, atomic force microscopy measurements showed a large step height between the poly- and single crystal CdTe

regions. Another proposed structure for QPM consists of alternating <i00>/<111> stripes of CdTe. We can grow <100>CdTe on a GaAs surface that has a native oxide, and <111>CdTe on a clean GaAs surface. We are testing the use of AlGaAs layers as a means of controlling the orientation of the CdTe. Initial results with a high Al fraction yielded polycrystalline rather than <100> CdTe. During the next quarter we plan to investigate optimization of the Al fraction and *in-situ* preclean to obtain <100> material. (Gibbons, Fejer)

High Speed Optical Modulators and Measurements

We have been investigating the strained InGaAs/GaAs material system for improvement in our electro-absorption modulators. In the possible areas optical computing, processing, and interconnect applications, the strained InGaAs material is expected to be particularly useful since the substrate is transparent at the operating wavelength and there are efficient laser light sources available. Mathematical models of exciton wavefunctions predicted improvement in the quantum well absorption if the barrier height is incresaed by the addition of aluminum to the barriers. Conventionally, the AlGaAs/InGaAs material is considered poor for optical devices, since the large number of surface states and traps decreases the radiative lifetime. However, since modulators rely on absorption rather than recombination, we postulated that these detrimental effects would be less important. These devices are now being grown and will be processed next quarter. (Harris)

Ultrafast Sampler

We measured a 2.0 ps total system response time for the photodiode/sampler, corresponding to a 3 dB bandwidth of 150 GHz. To our knowledge this is the fastest photodiode ever reported. The responsivity was 0.15 A/W which gives a 33% external quantum efficiency at 532 nm. A modelocked Nd:YAG laser with a fiber-grating pulse compressor and crystal doubler was used to generate 1.1 ps pulses. These were phase-locked to a reference that drove the sampler at an offset rate giving a 240 ps time window. The measured system response of 2.0 ps includes contributions from the photodiode response time, the sampler aperture time, the laser pulse duration, the residual laser timing jitter, and microwave synthesizer jitter. We estimate the photodiode response time to be 1.5 ps. (D. Bloom)

Vertical Cavity Lasers

Material for the topless laser was grown at the Sandia National Laboratory and characterized there by a student visiting from Stanford. The linewidth of previously grown surface emitting lasers was measured to be 65 MHz by heterodyning two lasers on a fast photodiode, and the variation of frequency with injection current indicates that electrical feedback may be used for linewidth narrowing. A high-reflection dielectric coating was applied to a sample of the topless material for testing. This sample lased with a threshold of 10^5 W/cm^2 indicating promise for the external cavity laser. (Sandia Laboratory)

CALIFORNIA INSTITUTE OF TECHNOLOGY

Lattice Mismatch Accommodation by Ion-Assisted Molecular Beam Epitaxy

Progress and results of our investigation of lattice mismatch accommodation by ion-assisted molecular beam epitaxy (IAMBE) are described. In the last quarter, we investigated a novel scheme for lattice mismatch accommodation between Si and GaAs by reduction of dislocation density in fully-relaxed Ge buffer layers on Si, in order to provide a high-quality lattice-matched substrate for GaAs/Si heteroepitaxy. The new method involves confinement of misfit dislocations in relaxed Ge buffer layers by growth of epitaxial films rich in point-like defect on

the relaxed buffer layers. We have found that the layer containing point-like defects generated by IAMBE can actually confine misfit and threading dislocations within the relaxed buffer layer, leading to an order of magnitude reduction in dislocation density in layers grown *on* the IAMBE film with respect to the relaxed buffer layer *below* the IAMBE film.

To date, the best dislocation density achieved in 0.5 μm thick relaxed Ge films is $10^7/cm^2$. We note that this is already comparable to the best reported dislocation densities reported for Ge or GaAs films of this thickness grown at conventional MBE temperatures (200 - 550°C). Optimization of the dislocation density by adjusting defect concentration, growth temperature and buffer layer annealing temperature is underway.

Moreover, the IAMBE films containing point-like defects do not themselves act as sources of dislocations and stacking faults. A simple model for the dislocation/point defect array interaction suggests that the mechanism for the reduced mobility of misfit and threading dislocations in the IAMBE-grown films is similar to solution hardening and precipitate hardening mechanisms observed in hardened steel alloys.

In the upcoming quarter, we plan to begin growth of GaAs on relaxed Ge buffer films on Si, and to assess their quality relative to GaAs/Si grown by conventional techniques. Efforts will be devoted to improving the dislocation density in relaxed IAMBE Ge films to $10^6/cm^2$ in *thin* (<1 μm thick), *low temperature-grown* films (<600°C), in order to develop a GaAs/Si heteroepitaxy process, which is truly compatible with Si VLSI.

During the last quarter a cryopump was installed on our MBE system in order to improve the pumping speed for water and hydrogen. Delivery of an electron cyclotron resonance (ECR) ion source for ultra-low energy IAMBE experiments is scheduled for August 1991. (Harry A. Atwater)

Nanometer-Scale Selective Growth of GaAs and InGaAs by OMVPE and Application to Quantum Size Effect Semiconductor Lasers

There is currently great interest in the fabrication of structures that are two and three dimensional analogs of the conventional quantum well. Several potential applications of arrays of such structures have been proposed, including diode laser active layers and new nonlinear optical materials. Key problems involved in successfully applying these structures in devices are interface quality and abruptness, structural uniformity, and, for application to lasers, ability to efficiently pump the structures without leakage effects dominating. Selective growth is a potential candidate for fabricating highly uniform nanostructures and for providing extremely good built-in current blocking capability which could be exploited in ultra-low threshold conventional quantum-well laser diodes.

In order to perform nanometer-scale selective growth of GaAs using the special OMVPE precursor diethylgallium chloride (DEGaCl), an OMVPE reactor located at the NASA Jet Propulsion Laboratory has been allocated for modification to accommodate the DEGaCl precursor. The layout for the necessary modifications has been designed. The DEGaCl source and the necessary components for the modification, such as a mass flow controller, a temperature controlled thermal bath, and various valves, have been purchased.

A novel phase-sensitive lock-in-amplifier-based spectrally-resolved cathodoluminescence imaging system for analysis on nanometer scale structures at room, liquid nitrogen, and liquid helium temperatures has been developed and tested. The performance of this novel imaging system has been confirmed by analyzing GaAs, InGaAs, and AlGaAs materials grown by conventional OMVPE and molecular beam epitaxy (MBE).

Thin film (200Å) deposition and patterning processes for silicon nitride, the masking material used in selective growth, have been calibrated and optimized. Silicon nitride layers have been grown on bulk GaAs and OMVPE growth substrates by plasma enhanced chemical vapor deposition. Test patterns have been etched into the silicon nitride layers by conventional photolithographic process followed by reactive ion etching in a CF_4 plasma.

The OMVPE reactor modifications necessary to accommodate the DEGaCl precursor will be completed and safety tested. The new DEGaCl precursor will be installed and tested in the OMVPE reactor. Crystalline quality of materials from the initial GaAs growths at atmospheric pressure using the DEGaCl precursor and arsine will be checked by spectrally-resolved cathodoluminescence analysis.

The effect of mask opening orientation on the morphology and faceting properties of selectively grown GaAs structures will be investigated by scanning electron microscopy. AlGaAs barrier layers grown by conventional OMVPE will be calibrated by spectrally-resolved cathodoluminescence analysis. And finally, selective growth of multiple layer GaAs-AlGaAs heterostructures will be attempted. (Kerry J. Vahala)

Ultra-low Threshold Semiconductor Lasers

To minimize the power consumption of semiconductor lasers to a level that is useful for large scale integrated optoelelectronic circuits, it is important to reduce the threshold current below 1 mA. Quantum well lasers have demonstrated an order of magnitude reduction in laser threshold over bulk materials, with the best threshold currents at around 0.5 mA. Still, theoretical considerations predict that a factor of 5 lower values should be achievable with existing technology. A further reduction in laser threshold, by nearly a factor of 2, is predicted when using a strained InGaAs quantum well active layer. To date we have measured threshold currents as low as 0.75 mA (CW) in strained InGaAs/AlGaAs quantum well lasers.

From theoretical estimates and measurements on bulk laser material it can be shown that semiconductor laser threshold currents can be reduced an order of magnitude by lowering the operating temperature to 5 K. The ultimate threshold limit with existing devices will then fall below 100 mA. In practical systems, this is easily achieved in spacecraft and antennas where often other devices and circuitry are already at cryogenic temperatures.

We have studied the operation of ultra-low threshold current buried heterostructure (BH) GaAs and strained InGaAs quantum well lasers from room temperature down to 5 K [1]. Our best available devices had threshold currents of 4.5 mA (GaAs) and 1.1 mA (InGaAs) at room temperature. We find that below 200 K the threshold decreases linearly with temperature for both types of lasers [Figure 1]. We have measured a minimum threshold current of 120 mA (!) for the GaAs laser and 165 mA for the InGaAs laser at 5 K. We notice a difference in slopes, dI_{th}/dT, between the InGaAs and GaAs lasers, with the GaAs threshold decreasing 2.5 times faster with temperature. We have explained this difference by a simple model, which only takes into account the lower valence band effective mass for the strained InGaAs material.

Although lower transparency current densities have been measured in our InGaAs materials, this has not yet resulted in lower room temperature threshold currents in the final BH lasers. To optimize these devices we are studying the trade-offs between available gain (i.e. number of

---

[1] L.E. Eng, A. Sa'ar, T.R. Chen, I. Grave, N. Kuze, and A. Yariv " Microampere Operation of GaAs and Strained InGaAs Quantum Well Lasers at Low Temperatures (5K)", *Appl. Phys. Lett.* **58** (24), (1991).

quantum wells, gain per well), at a given current, and the required threshold gain (mirror and internal losses).

The lasers used for the low temperature measurements are not optimized devices at room temperature. We intend to repeat the measurements with better devices and futher to investigate carrier lifetimes and laser dynamics. (A. Yariv)

Massively Parallel Optical Networks

The demonstration of a massively optically interconnected parallel network critically depends on the availability of a two-dimensional array of optical switches, which provide the nonlinear operation necessary to achieve the function of the network. This nonlinear operation can be easily implemented in GaAs optoelectronic integrated circuits because variety of optical and electronic devices can be monolithically integrated in GaAs. One version of the neurons implemented in GaAs is using double-heterojunction bipolar transistors coupled with a light-emitting diode (LED). Because of the high optical gains needed in these switches, these transistors need to draw tremendous current in order to satisfy this requirement. Thus, heat dissipation becomes a severe limitation in extending these switches to large arrays. Consequently, alternative integration schemes based on metal-semiconductor field-effect transistors (MESFETs) are explored. In addition, a new circuit incorporating input and output isolation is investigated. The results on these new neurons provide optimism towards implementing these switches in large arrays. In this report, specific accomplishments in the development of new optoelectronic integrated switches are presented, along with clear statements of the tradeoffs for using bipolar transistors and MESFETs in implementing these switches. It is hoped that through further research, the characteristics of the switches can be improved and the density can be greatly increased.

The implementation of bipolar transistors in integrated optoelectronic switches involves optimization of current gains in these transistors. For a typical bipolar transistor, its current, β, is dependent upon the current through the transistor in a roughly square root fashion. Because of the inherent optical losses due to the low diffraction efficiency in the optical interconnection medium, these switches have to manifest large internal optical gains so that signals transmitted from one plane to the next would not decay. Switches utilizing this design have shown an overall optical gain of 20. However, the electrical power dissipation is about 100 mW/switch, which severely limits the density of the array in the future if we are to continue using bipolar transistors as the driver of LED in optoelectronic switching elements. For this reason, MESFET-based integrated optoelectronic switches have been developed.

The schematic circuit diagram for the MESFET-based switches is shown in Fig. 1. This new circuit is composed of an output circuit made of a MESFET driving the LED and an input circuit, which incorporates a bipolar phototransistor as the light detector and another MESFET as its active load. LEDs are chosen as the light source, as opposed to lasers, because no threshold currents are needed to drive the LEDs so that a large array of optoelectronic switches at low currents can be built. With sufficient light incident on the phototransistor, the phototransistor pulls up the voltage, V_o, which is also the gate voltage of the output driving MESFET. This increase in this voltage turns on the output MESFET, and the current drawn by the transistor drives the LED. The treshold of the switch can be electrically controlled by a bias voltage, V_B, applied to the gate of the loading MESFET, which provides the reference current to be compared with the photocurrent generated by the incident beam.

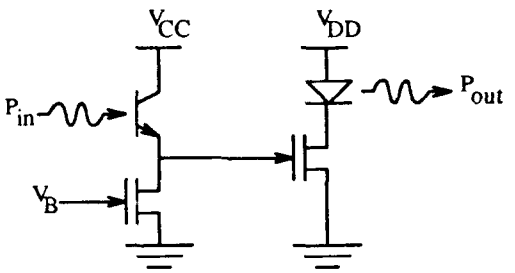

Fig. 1 Schematic Circuit Diagram of an Optoelectronic Switch Incorporating MESFETs as the Driver for the LED

This design has several advantages over the previous one. The most distinct advantage is the employment of MESFETs, which are voltage-driven devices, as opposed to bipolar transistors, which are current-driven devices. Because of this difference, the gate voltage of the LED-driving MESFET can be charged up by a separate switching circuit, which is totally isolated from the main circuits, thus achieving a total input-output isolation. This can not be done in bipolar transistors because the base current generated by the input beam is amplified directly to drive the LED. Thus, the input and the output are strongly coupled. Furthermore, the input switching circuit that controls the output circuit can be separately optimized for its sensitivity and switching characteristics. This may not be possible with bipolar transistors because the same transistor that detects the lights is acting as a signal amplifier at the same time. Thus, the superior properties of this circuit dramatically increase the flexibility on the design of the switch.

Fig. 2 shows the measured input-output characteristics of an optoelectronic switch. For the curve, V_B = -3V, a differential optical gain of 6 has been measured in the switch, which is limited by the leakage currents across the gate-drain schottky diodes in both MESFETs as well as the finite output conductances of the phototransistor and the loading MESFET. The leakage current across the gate-drain in the loading MESFET also limits the minimum power needed to the turn on the switch to 3 μW. When characterized individually, the LED and the phototransistor exhibit efficiencies of 0.01 W/A and 1 A/W, respectively. The transconductances of the MESFET's g_m, is measured to be 20 mS/mm. The current through the LED is about 1.2 mA, which implies, with V_{DD} = 2 V, the electrical power dissipation per switch is about 2.4 mW. The rise time of the switch is measured to be 5 μsec, and is found to be limited by the charging of the capacitors in the circuits. With these results, the optical switching energy per switch is thus calculated to be (2 μW) x (5 μsec) =10 pJ. Though an

optical gain of only 6 is obtained, the electrical power dissipation has been reduced down to only 2.4 mW/switch, which is impossible for switches that incorporate surface-emitting lasers as light sources. This represents a factor of 55 reduction in power dissipation when compared to the bipolar transistor switches. It is expected by further reducing the size of the transistors and the leakage currents the optical gain will improve along with the reduction in the optical switching energy and electrical power dissipation. These improvements are necessary if large arrays of optoelectronic neurons are to be practically incorporated into a neural network system in the future. (D. Psaltis)

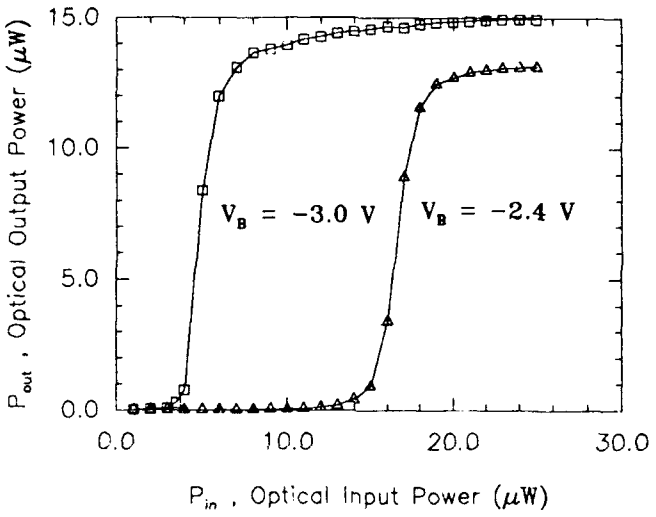

Fig. 2 Measured Input-Output Characteristics of the MESFET-based Optoelectronic Switch

SPIE Proc. Vol. 1418 - Laser Diode Technology and Applications III (D. Renner, Ed.), OE/LASE '91, Los Angeles, CA, 20-25 Jan. 1991

VERTICAL-CAVITY SURFACE-EMITTING SEMICONDUCTOR LASERS: PRESENT STATUS AND FUTURE PROSPECTS

(Invited paper)

Marek Osiński*

Center for High Technology Materials, University of New Mexico, Albuquerque, New Mexico 87131-6081

ABSTRACT

A dramatic progress in the development of high-quality vertical-cavity surface-emitting lasers (VC-SELs) has been achieved during the last coupie of years, with very strong contributions made by U.S. researchers. In particular, new concepts of microlasers and resonant-periodic-gain devices have been proposed and implemented, and devices with strained-quantum-well active regions have been demonstrated. This paper reviews the present status and future prospects for (VC-SELs), with emphasis on recent developments in the U.S.

1. INTRODUCTION

Vertical-cavity surface-emitting lasers (VC-SELs) have a unique history of long and painstaking development by a single research group, in the atmosphere of prevailing skepticism reigning in the semiconductor laser community. For over a decade since their invention in 1977, development and studies of vertical-cavity surface-emitting lasers (VC-SELs) have been limited to a single group at Tokyo Institute of Technology, led by Kenichi Iga [Iga 1988]. The apparent lack of interest in VC-SELs amongst semiconductor laser researchers was caused by notoriously poor performance of those devices (high threshold currents, low efficiencies, no cw operation at room temperature). For example, as recently as in 1988 the pulsed room-temperature threshold current densities were ~30 times larger than the corresponding cw densities in edge emitting lasers [Sakaguchi 1988]. Until very recently, VC-SELs have not even been seriously considered for any applications. This situation has changed dramatically over the last couple of years, during which a startling progress in the development of high-quality VC-SELs has been achieved. In this paper, we will examine the present status and future prospects for VC-SELs, with emphasis on recent advances in the U.S. Parallel developments in Japan are described elsewhere in this volume [Ogura 1991].

An important driving force behind the recent surge of interest in VC-SELs is a wide range of potential applications for two-dimensional (2-D) laser arrays. While individual VC-SELs may represent an alternative to existing edge-emitting lasers, they offer unique novel opportunities when assembled into 2-D arrays. Compared to conventional arrays of grating surface emitters or deflected-beam diode lasers, VC-SEL arrays offer the advantages of high packing density, larger emitting areas and consequently higher output power, unconstrained arrangement of emitters, wafer-scale processing, inherent single-longitudinal-mode operation, and narrow nearly-circular output beams that facilitate coupling to optical fibers or redirection and detec-

* Also with the Department of Electrical and Computer Engineering and the Department of Physics and Astronomy, University of New Mexico.

tion in open-space systems. Compatibility with vertical stacking architecture allows to integrate these arrays into more complex system. Moreover, large numbers of VC-SELs with each emitter having a different wavelength can be integrated monolithically [Chang-Hasnain 1990b], [Chang-Hasnain 1991]. These features render them ideal for many new applications, such as chip-to-chip communications, free-space optical communications, optical recording, medicine, *etc.* Especially attractive are applications requiring high degree of parallelism, such as optical interconnections, optical computing, image processing, and optical pattern recognition.

Replacement of electrical interconnections with optical devices has many potential advantages such as high interconnection densities, high transmission speed, low power requirements, low loss, low dispersion, low mutual interference, immunity to RFI, EMI, and EMP, and reduced impedance matching and groundplane requirements [Goodman 1984], [Feldman 1988]. Both free-space and guided-wave configurations can be used. The successful implementation of optical interconnections in real systems largely depends, however, on the development of suitable two-dimensional arrays of low cost, high speed, high packing density, reliable optical sources that would operate at low driving currents and would deliver sufficient output power.

2. CLASSIFICATION OF VC-SEL STRUCTURES

Dramatic progress in VC-SELs over the last two years brought forth a variety of novel device structures. Conventional VC-SELs had bulk, double-heterostructure active regions. A typical geometry of etched-well ring-contact cylindrical structure is shown in Fig. 1. Recent development efforts concentrated on reducing the lasing threshold and/or increasing the maximum output power. Significant new concept was replacement of the bulk active region with narrow (single- or multiple-quantum-well) layers in a carefully designed cavity such that the position of the active layer would coincide with an antinode of laser radiation at a designed wavelength of operation. VC-SELs with a single active region satisfying this resonant condition are often called microlasers [Jewell 1989b], [Jewell 1990a] (see Fig. 2). A simple extension of the microlaser concept leads to introduction of distributed-Bragg-reflector resonant-periodic-gain (DBR-RPG) lasers [Raja 1989], [Corzine 1989b] (Fig. 3), in which multiple active regions are separated by half-wave spacers. The most recent advance in RPG laser structures is a distributed-feedback resonant-periodic-gain (DFB-RPG) VC-SEL [Mahbobzadeh 1990] (Fig. 4), where an RPG active region is intercalated with the multilayer reflectors.

A characteristic feature of VC-SELs that distinguishes them from edge-emitting semiconductor lasers is their small single-pass gain, reminiscent of gas lasers. As a direct consequence of small gain, in order to avoid prohibitively high lasing threshold it is necessary to place the active medium in a high-Q resonator. In today's state-of-the-art VC-SELs, this is almost invariably achieved by providing a Bragg resonator consisting of a stack of high-reflectivity quarter-wave layers on either side of the active medium.

3. PROGRESS IN PERFORMANCE OF VC-SELS

3.1. Threshold

Due to extremely short length of the active medium, it is imperative to achieve very high (close to unity) reflectivities of the mirrors defining the Fabry-Pérot resonator. Several concepts were employed to reach that goal: quarter-wave dielectric multilayer reflectors [Zinkiewicz 1989], [Yoo 1990], quarter-wave semiconductor multilayer reflectors [Jewell 1989a], [Scherer 1989], metallic reflectors [Deppe 1989], [Yang 1990], [Schubert 1990], [Tu 1990] and hybrid mirrors, combining semiconductor and metallic reflectors [Schubert 1989], [Fisher 1990] or semiconductor and dielectric layers [Ho 1990a]. The high reflectivity semiconductor mirror

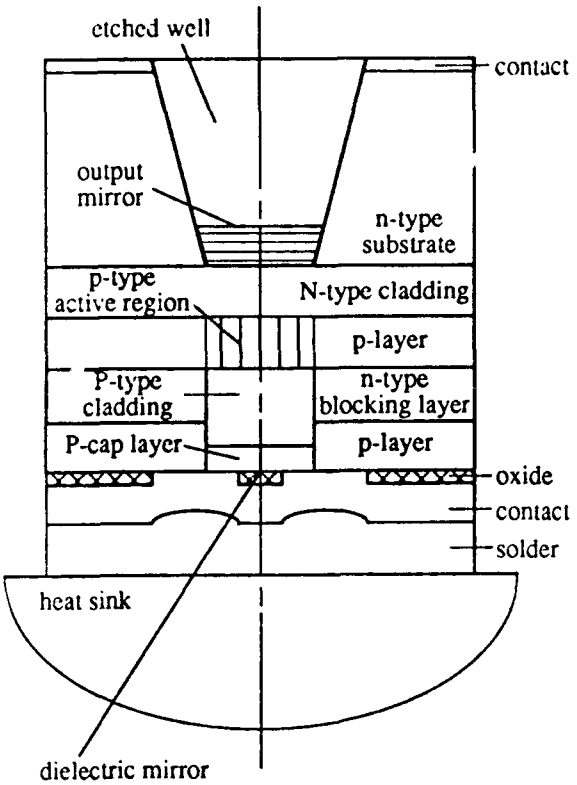

Fig. 1. Typical geometry of a conventional etched-well VC-SEL.

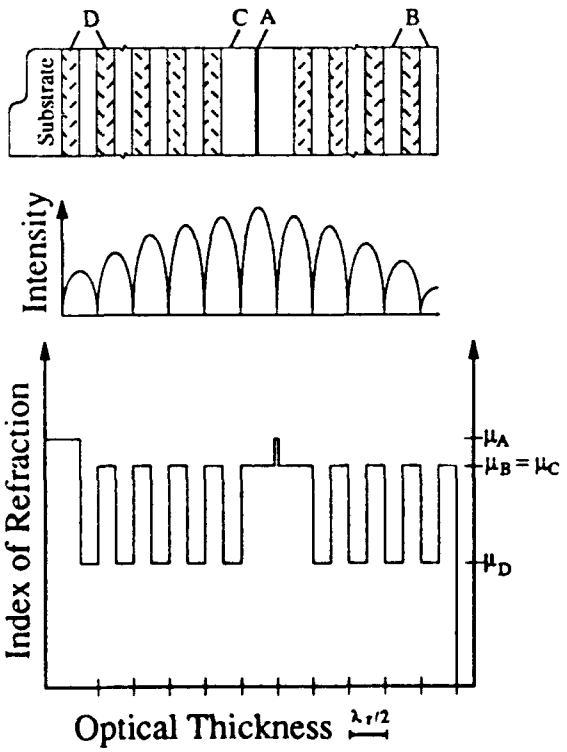

Fig. 2. Schematic illustration of layer structure, optical intensity distribution, and refractive index profile in a microlaser. Thick line (A) represents high-index quantum-well active layer, unshaded regions (B) - intermediate-index quarter-wave spacers, unshaded regions (C) - intermediate-index half-wave spacers, shaded regions (D) - low-index quarter-wave spacers.

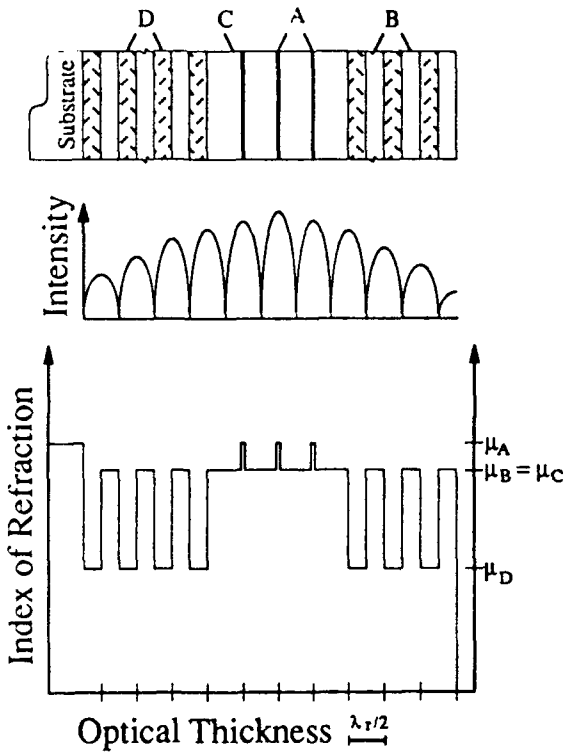

Fig. 3. Schematic illustration of layer structure, optical intensity distribution, and refractive index profile in a DBR-RPG laser. Layer designation is the same as in Fig. 2.

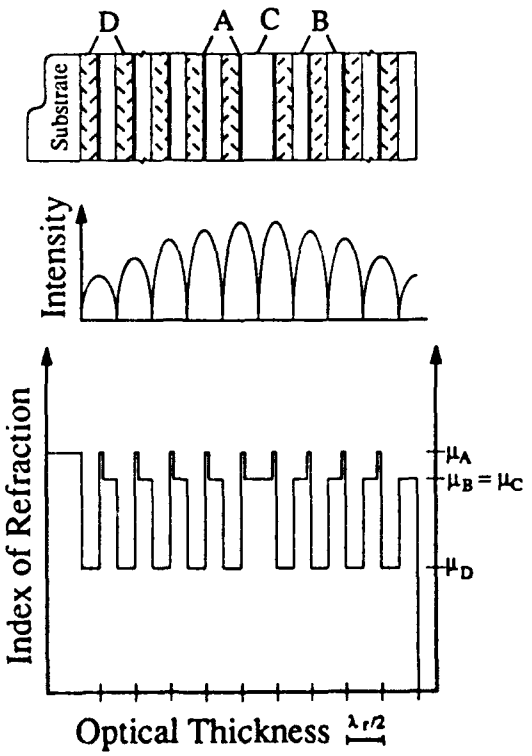

Fig. 4. Schematic illustration of layer structure, optical intensity distribution, and refractive index profile in a DFB-RPG laser. Layer designation is the same as in Fig. 2.

growth represents a significant technological challenge, since it requires a very good control of each layer thickness and composition. Calculations indicate that changing the thickness in one quarter-wave layer by only one unit cell (two monolayers) produces a shift of resonant wavelength up to 0.12 nm [Weber 1990]. In addition, rough interfaces reduce the reflectivity, introduce scattering and diffraction loss, and deform the wavefront of the lasing mode. Advanced crystal growth techniques, such as atomic layer epitaxy or phased-locked epitaxy [Walker 1990] may be utilized to provide ultimate perfection and uniformity of DBR layers with high reproducibility. Improved quality of interfaces can also be achieved by employing misoriented substrates [Wang 1990b].

Over the last two years, lasing threshold of VC-SELs for room-temperature operation has been reduced by orders of magnitude. The progress achieved in electrically pumped GaAs/AlGaAs devices is illustrated in Tables I and III for pulsed and cw operation, respectively.

So far, there have been relatively few reports of temperature dependence of lasing threshold. The characteristic temperature T_0 for pulsed threshold, given in Table II, is comparable to edge-emitting devices. However, as shown in Table IV, T_0 becomes significantly smaller for cw operation. Large difference between pulsed and cw values of T_0 indicates that strong temperature dependence of cw threshold in VC-SELs is primarily caused by thermal effects.

Optical pumping provides a convenient tool for studying VC-SEL structures. It can be used to evaluate potential performance of novel designs prior to achieving electrical pumping. It is worthwhile noting, however, that caution should be exercised when interpreting optical pumping data. With optical pumping, the active region is defined simply by the spot size of the pump beam, without any wafer processing. In electrically pumped structures, good confinement of carriers in columnar devices is accompanied by increased surface recombination at side walls, while planar structures suffer from current spreading. Hence, the threshold current density estimated from optical pumping data [Jewell 1989b] may lead to overoptimistic conclusions.

Another point of caution when interpreting the optical pumping results is a considerable uncertainty in evaluating the pump power actually absorbed in the active region. This somewhat corresponds to difficulties in establishing the pumping current in the active region in the presence of current spreading.

Tables V and VI contain data on room-temperature lasing threshold in optically pumped VC-SELs under pulsed and cw conditions, respectively.

3.2. Output power and efficiency

In evaluating progress in VC-SELs with respect to output characteristics, we have selected peak output power and overall power conversion efficiency as the main indicators. We have not included the slope efficiency η_d, since it can be made artificially high by reducing mirror reflectivities at the expense of increased threshold current. For example, η_d can be increased from ~15% to 54% by reducing the Ag mirror thickness from 400 Å to 300 Å [Tu 1990]. However, in the same instance, the pulsed threshold current density j_{th} in 20-μm diameter devices increases from 13 to 19 kA/cm^2 (I_{th} raising from 40 to 60 mA).

Tables VII and VIII contain data on output power and energy conversion efficiency for electrically-pumped VC-SELs operating under pulsed and cw conditions, respectively. Optical pumping results are summarized in Tables IX and X.

Table I. Room Temperature Pulsed Threshold

j_{th} [kA/cm^2]	I_{th} [mA]	V_{th} [V]	t_p [ns]	η_p [%]	Size [μm]	Structure	Reference
26	250		200	0.02	35 Ø	3 μm DH-DBR	[Zinkiewicz 1989]
25	20	1.3	100	1	10 Ø	0.6 μm DH-DBR, 400 Å Ag mirror	[Tu 1990]
18.4	1.3	15	50		3 Ø	unpassivated 3x8 nm MQW strained columnar μlaser	[Jewell 1989c]
16	115				30 Ø	0.7 μm DH-DBR 550 nm Ag mirror	[Deppe 1989]
15.3	12				10 Ø	0.5 μm DH-DBR	[Fischer 1990]
14.7	26				15 Ø	0.25 μm ion-implanted DH-DBR	[Tai 1989a]
14	16		200	2	12 Ø	20x15 nm GRINSCH-MQW-DBR	[Wang 1990a]
10.6	12	3.5	200	2	12 Ø	0.47 μm DH-DBR misoriented substrate	[Wang 1990b]
10.4	130		200	0.02	40 Ø	0.6 μm DH-DBR	[Botez 1989]
10.2	2	8	50		5 Ø	unpassivated 3x8 nm MQW strained columnar μlaser	[Jewell 1989c]
5.6	1.1		90		5 Ø	unpassivated 10nm SQW strained columnar μlaser	[Lee 1989]
3.2	3.2	4.2	100	2	10x10	3x8 nm MQW strained ion-implanted μlaser	[Lee 1990a]
2.3	45		90		50 Ø	unpassivated 10 nm SQW strained columnar μlaser	[Lee 1989]
1.9	7.5	10	300	0.3	20x20	3x8 nm MQW strained columnar μlaser	[Chang-Hasnain 1990a]
1.4	10.2		150	1	30 Ø	4x10 nm MQW proton-implanted μlaser	[Lee 1990b]
1.25	5	3.5	300	0.3	20x20	3x8 nm MQW proton-impanted strained μlaser	[Chang-Hasnain 1990a]
1.22	6		400	0.2	25 Ø	strained μlaser	[Yoo 1990b]
1.1	17	3	200	0.2	40x40	3x8 nm MQW proton-implanted strained μlaser	[Orenstein 1990]
0.74	3				20x20	strained columnar μlaser	[Clausen 1990]
0.6	26.5				75 Ø	8 nm SQW strained columnar μlaser	[Geels 1990a]

j_{th} - threshold current density
I_{th} - threshold current
V_{th} - threshold voltage
t_p - pulse length
η_p - duty cycle

Table II. Characteristic Temperature T_o for Pulsed Operations

T_o [K]	Range [°C]	Size [μm]	Structure	Reference
210	10-90	15 Ø	4x10 nm MQW GRINSCH proton-implanted μlaser	[Hasnain 1990]

T_o - characteristic temperature

Table III. Room Temperature CW Threshold

j_{th} [kA/cm^2]	I_{th}[mA]	V_{th} [V]	Size [μm]	Structure	Reference
130	2.3	27	1.5 Ø	unpassivated 3×8 nm MQW strained columnar μlaser	[Jewell 1990b]
31.8	1		2 Ø	passivated 3×8 nm MQW strained columnar μlaser	[Jewell 1990b]
22.6	40		15 Ø	0.5 μm DH-DBR	[Tai 1989b]
19.6	8		8 Ø	metallic mirror 0.6 μm DH-DBR	[Schubert 1990]
9.4	24	1.8	18 Ø	metallic mirror 0.6 μm DH-DBR	[Schubert 1990]
9.4	1.5		4×4	2 μm DH-DBR	[Hsin 1990]
6.6	2.5		7 Ø	3×8 nm MQW strained columnar μlaser	[Jewell 1990b]
6	1.5		5×5	10 nm SQW strained columnar μlaser	[Jewell 1990b]
4.1	0.8		5 Ø	passivated 3×8 nm MQW strained columnar μlaser	[Jewell 1990b]
3.6	3.6	3.7	10×10	3×8 nm MQW strained ion-implanted μlaser	[Lee 1990a]
2.8	2.2	7.5	10 Ø	4×10 nm MQW proton-implanted μlaser	[Lee 1990b]
1.4	0.7	4	7×7	8 nm SQW strained columnare μlaser	[Geels 1990b]
1.2	4.8		20×20	strained columnar μlaser	[Clausen 1990]
1.1	7.5	4	30 Ø	4×10 nm MQW proton-implanted μlaser	[Tell 1990]
0.8	1.1	4	12×12	8 nm SQW strained columnar μlaser	[Geels 1990a]

j_{th} - threshold current density
I_{th} - threshold current
V_{th} - threshold voltage

Table IV. Characteristic Temperature T_0 for CW Operation

T_0 [K]	Range [°C]	Size [μm]	Structure	Reference
115	15-50	15 Ø	0.5 μm DH-DBR	[Tai 1989b]
130	10-50	15 Ø	4×10 nm MQW GRINSCH proton-implanted μlaser	[Hasnain 1990]

T_0 - characteristic temperature

4. PERFORMANCE OF CONVENTIONAL VC-SELs

Conventional VC-SELs with thick active regions carry a potential for high-power operation, with the highest reported pulsed output power of 120 mW emitted by devices with diameter of 35 μm [Zinkiewicz 1989]. The cw output is however considerably lower, with thermally

limited light-output characteristics exhibiting a downward bend at output power levels near 1 mW for etched-well devices [Tai 1989b].

As recently as two years ago, the pulsed room-temperature threshold current densities of VC-SELs were ~30 times larger than the corresponding cw densities in edge emitting lasers [Sakaguchi 1988]. The threshold in conventional VC-SELs remains, however, very high (about 10 kA/cm^2 [Botez 1989], [Schubert 1990], compared to less than 1 kA/cm^2 in GaAs/AlGaAs edge emitters with similar bulk active regions), which indicates that thermal effects are still critical.

Conventional planar VC-SELs have been successfully integrated into closely packed phased-locked arrays [Deppe 1990], [van der Ziel 1990]. However, the familiar double-lobed far-field pattern that plagues the high-power edge-emitting phased arrays has been observed. Hence, one of the major attractions of VC-SELs which is its circular narrow output beam is lost when high-order 2-D supermodes are excited [Yoo 1990c]. It can be expected that achievement of stable single-lobe far-field in 2-D arrays will represent a formidable challenge.

Table V. Room-Temperature Pulsed Threshold - Optical Pumping

p_{th}[kW/cm^2]	P_{th} [mW]	t_p [ns]	η_p [%]	Size [μm]	Structure	Reference
50900*	900*	0.01	0.08	1.5 Ø	1.6 μm DH-DBR	[Jewell 1989a]
1,600	1,250	12		10 Ø	150x10 nm MQW-DBR	[Gourley 1987]
820	410	0.01	0.08	8 Ø	20x8 nm strained MQW DBR	[Huang 1989]
30	24			10 Ø	20x60 nm DBR-RPG	[Corzine 1989b]
17.5	86	7	10^{-6}	25 Ø	20x10 nm hybrid DFB-DBR RPG	[Schaus 1989]

p_{th} - threshold irradiance (absorbed)
P_{th} - threshold pump power (absorbed)
t_p - pulse length
η_p - duty cycle
* - incident irradiance and power

Table VI. Room-Temperature CW Threshold - Optical Pumping

p_{th}[kW/cm^2]	P_{th} [mW]	Size [μm]	Structure	Reference
0.7	1.5	20 Ø	8 nm SQW strained μlaser	[Jewell 1989b]

p_{th} - threshold irradiance (absorbed)
P_{th} - threshold pump power (absorbed)

Table VII. Room Temperature Pulsed Output Characteristics

p [kW/cm^2]	P_{max} [mW]	η [mW/mA, %]	t_p [ns]	η_p [%]	Size [μm]	Structure	Reference
0.28	0.4		500		12×12	8 nm SQW strained columnar μlaser	[Geels 1990a]
0.57	25				75 Ø	8 nm SQW strained columnar μlaser	[Geels 1990a]
0.75	3	0.16, 12			20×20	strained columnar μlaser	[Clausen 1990]
1.4	4.5	0.07, 5.0	100	1	20 Ø	0.6 μm DH-DBR, 3000 Å Ag mirror	[Tu 1990]
2.7	2.2	0.12, 9.4			9×9	strained columnar μlaser	[Clausen 1990]
2.7	3	0.07, 5.1	200	2	12 Ø	20×15 nm GRINSCH-MQW-DBR	[Wang 1990a]
2.8	45	0.07, 5.2	200	0.2	40×40	3×8 nm MQW proton-implanted strained μlaser	[Orenstein 1990]
5.3	6	0.12, 8.3	200	2	12 Ø	0.47 μm DH-DBR misoriented substrate	[Wang1990b]
12.5	120	0.11, 7.8	200	0.02	35 Ø	3 μm DH-DBR	[Zinkiewicz 1989]
14	11	0.14, 9.8	100	1	10 Ø	0.6 μm DH-DBR 400 Å AG mirror	[Tu 1990]
46.7	18				7 Ø	3×8 nm MQW strained columnar μlaser	[Jewell 1990b]

p - power density
P_{max} - maximum power
η - overall efficiency
t_p - pulse length
η_p - duty cycle

Table VIII. Room Temperature CW Output Characteristics

p [kW/cm^2]	P_{max} [mW]	η [mW/mA, %]	Size [μm]	Structure	Reference
0.31	0.55	0.10, 6.9	15 Ø	4×10 nm GRIN-SCH proton-implanted μlaser	[Hasnain 1990]
0.45	3.2	0.12, 8.3	30 Ø	4×10 nm GRIN-SCH proton-implanted μlaser	[Tell 1990]
0.68	1.2	0.02, 1.2	15 Ø	0.5 μm etched-well DH-DBR	[Tai 1989b]
0.70	0.7	0.06	10×10	3×8 nm MQW strained ion-impanted μlaser	[Lee 1990a]
0.76	0.6	0.11, 7.4	10 Ø	4×10 nm MQW proton-impanted μlaser	[Lee 1990b]
0.78	0.3	0.05, 3.9	7 Ø	3×8 nm MQW strained columnar μlaser	[Jewell 1990b]
1.91	1.5	0.21, 14.5	10 Ø	4×10 nm GRIN-SCH proton-implanted μlaser	[Tell 1990]

p - power density
P_{max} - maximum power
η - overall efficiency

Table IX. Room-Temperature Pulsed Ouput Characteristics - Optical Pumping

p [kW/cm^2]	P_{max} [mW]	η [%]	t_p [ns]	η_p [%]	Size [μm]	Structure	Reference
12.4	61	6.1	7	10^{-6}	25 Ø	20x10 nm hybrid DFB-DBR RPG	[Schaus 1989]

p - output power density
P_{max} - maximum power
η - overall efficiency
t_p - pulse length
η_p - duty cycle

Table X. Room-Temperature CW Output Characteristics - Optical Pumping

p [kW/cm^2]	P_{max} [mW]	η [%]	Size [μm]	Structure	Reference
56	40	36	10 Ø	60x10 nm DBR RPG	[Gourley 1989a]

p - output power density
P_{max} - maximum power
η - overall efficiency

5. PERFORMANCE OF MICROLASER VC-SELs

Strong interest in microlaser structures is to a large extent propelled by their relatively easy electrical pumping and capability of operating at low current levels. Originally, microlasers were fabricated in form of etched columns with side walls exposed to external environment. While this approach produces spectacular images [Lee 1989] and allows for a million of microlasers to be processed on a single wafer [Jewell 1990a], it is certainly not optimal from the point of view of reducing the threshold. In addition to very inefficient heat dissipation, surface recombination introduces a significant loss mechanism for structures of very small volume. In order to protect the etched columns from negative ambient influence, a buried-mesa geometry was proposed [Geels 1990a], in which the exposed surface is covered with polyimide (Fig. 5). Further improvement of device quality supplemented by a simplified fabrication process occurred with introduction of planar ion-implanted microlasers (Fig. 6) [Tai 1989a], [Tell 1990].

If the active region consists of a strained InGaAs/GaAs quantum well which radiates at a longer wavelength than GaAs, the output beam can be conveniently collected through a GaAs substrate without any necessity to etch a window. By the same token, reabsorption of laser emission in GaAs layers forming part of distributed Bragg reflectors can be greatly reduced.

Electrically pumped VC-SELs often suffer from increased threshold voltages caused by high series resistance of DBR reflectors, especially in the p-type doping case. Special precautions need to be taken to reduce excessive voltage drop at interfaces. An effective way to reduce height of barriers formed at abrupt interfaces is to utilize either short-period superlattices with gradually changing composition [Geels 1990a], [Tai 1990a] or "staircase" DBRs with additional intermediate bandgap layers [Tai 1990a]. The specific series resistance of conventional 10-period p-type GaAs/$Al_{0.7}Ga_{0.3}As$ DBRs (~7×10^{-3} Ωcm^2) can be reduced by as much as two orders of magnitude by introducing staircase DBRs (6.2×10^{-5} Ωcm^2) or superlattice DBRs (8.5×10^{-5} Ωcm^2) [Tai 1990a]. Even though peak reflectivity of staircase or superlattice DBRs is slightly re-

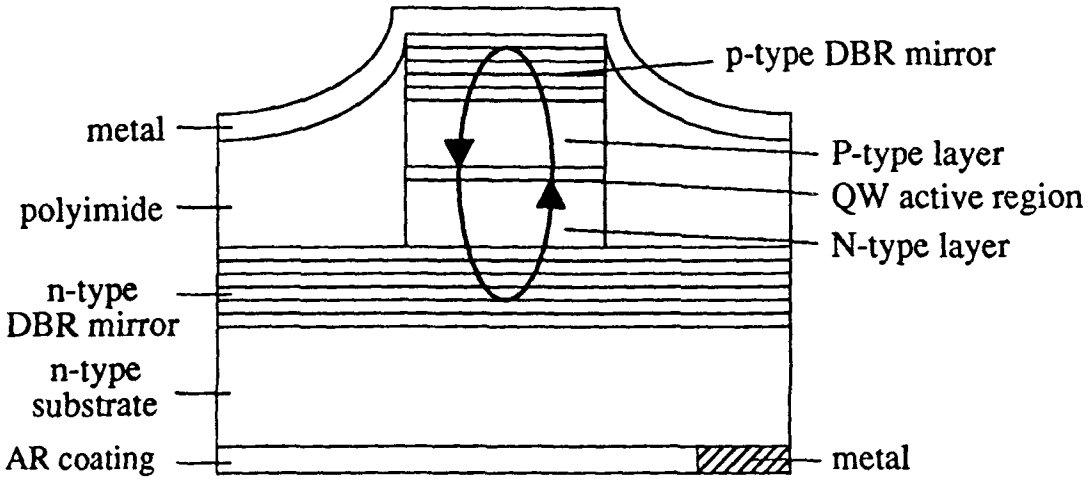

Fig. 5. Schematic illustration of a buried-mesa microlaser.

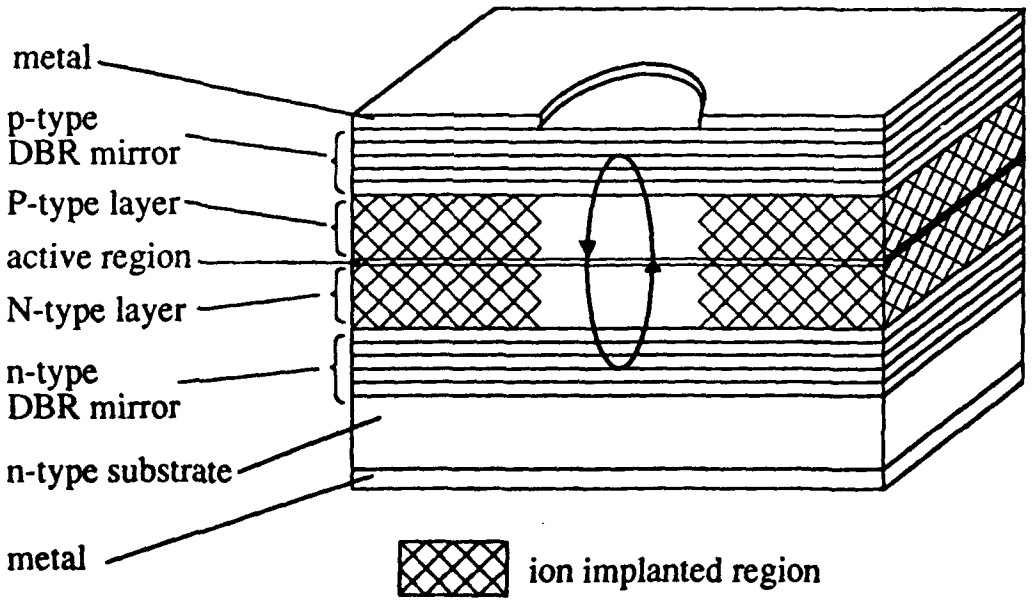

Fig. 6. Schematic illustration of a planar ion-implanted microlaser.

duced compared to quarter-wave DBRs, it is clear that even with one or two extra periods compensating for smaller reflectivity the series resistance will still remain very low. Staircase p-type DBRs have helped to reduce threshold voltages in gain-guided proton-implanted microlasers from 7-8 V to 3.7-4.2 V [Lee 1990c].

The highest reported cw output power from planar microlasers is 1.5 mW for 10-μm diameter GaAs/AlGaAs devices with four-quantum-well active region and over 3 mW for 30-μm diameter devices [Tell 1990]. It is important to note that although the emitting surface was increased ninefold, only twofold increase of the output power was achieved. This is a clear indication that the cw output was thermally limited and that the thermal problems deteriorate with increasing device diameter. The highest reported output power from columnar microlasers does not exceed 300 μW for a 7-μm diameter device with strained quantum well InGaAs/AlGaAs active region [Jewell 1990b].

Suitability of microlasers for fiber-optic applications has been demonstrated. Two-dimensional Gaussian-like transverse mode far field allow for much more efficient coupling into optical fibers than for conventional edge-emitting lasers. 50% butt coupling efficiency was measured for 8-μm core standard silica fibers with flat cleaved ends, and as much as 90% was achieved for fibers with etched lens-like ends [Tai 1990b]. This is the highest coupling efficiency ever reported for any diode laser. The best results obtained for edge-emitting lasers are in the range of 40-50% [Hillerich 1988]. Single-wavelength output with more than 50 dB side mode suppression ratio (again the highest ever reported), combined with 3-dB bandwidth exceeding 5 GHz [Hasnain 1990] clearly show that microlasers have reached the level of performance sufficient for first optical communication experiments to be attempted.

Coherent two-dimensional arrays of microlasers have been fabricated. Provided the size of individual emitters and their separation is sufficiently small, it is possible to maintain strong optical coupling between array elements. A phase-locked array comprised of 160 columnar microlasers of 1.3-μm diameter separated by less than 0.1 μm has been demonstrated [Yoo 1990a].

6. PERFORMANCE OF RPG VC-SELs

In parallel to microlasers, resonant-periodic-gain (RPG) structures have been pursued [Geels 1988], [Raja 1988a], [Raja 1988b], [Raja 1988c]. Both designs achieve gain enhancement in the vertical direction by aligning the active regions with the maxima of the longitudinal mode pattern at the designed wavelength, thus avoiding pumping the regions around the nulls of the standing wave. By the same token emission at non-resonant wavelengths is suppressed, and parasitic amplified spontaneous emission is reduced. Compared to microlasers, RPG structures carry a promise of generating higher output powers, by virtue of extended thickness of the active material. The alignment of peaks of an optical standing wave with quantum-well active layers leads to a significant reduction of the threshold current and additional enhancement of the maximum output power.

For VC-SELs, the total thickness of the device is of primary concern, since apart from issues of technological complexity and cost it also affects the ability to pump uniformly the device. First RPG structures were all of DBR type (see Fig. 3), with the total thickness significantly larger than the microlaser. Remarkable reduction of RPG laser thickness can be achieved by introducing, in analogy with edge-emitting lasers, a DFB-RPG structure [Mahbobzadeh 1990], shown in Fig. 4. The length of a DFB-type structure is inherently shorter than that of a DBR device with the same reflectivity of multilayer high reflector, because the amplifying and feedback sections overlap in the former structure whereas they are separated in the latter one. By replacing the DBR-RPG design with DFB-RPG, the total thickness of the device can be almost halved without compromising the characteristic features of RPG active medium. Compared

to present DBR-RPG structures, the DFB-RPG devices offer the advantages of considerably simpler fabrication process, improved wavelength selectivity, and strong discrimination against excitation of satellite longitudinal modes.

A slight modification of the structure shown in Fig. 4 results in a version of DFB-RPG VC-SEL that resembles a microlaser structure. Extending the length of the phase shifter to a full wave and placing an additional active layer in its center produces a microresonator sandwiched between two DFB sections, as indicated in Fig. 7. Compared to a usual microlaser structure, considerably higher output power can be obtained from the DFB-RPG laser, without any penalty whatsoever in the total device thickness. It should be noted, however, that the DFB-RPG structure of Fig. 4 is preferable to that of Fig. 7, since the latter contains one quantum well (symmetric quantum well in the center of the phase shifter) that is different from all the remaining ones.

So far, most experiments with RPG lasers involved optical pumping techniques. However, in order for these devices to reach their full application potential, it is necessary to develop an electrical pumping scheme. The substantial thickness of the RPG active region makes it very difficult to adopt the usual vertical pumping configuration without incurring a substantial penalty in threshold due to a non-uniform and inefficient carrier injection. On the other hand, transverse-junction pumping schemes do seem to represent a better approach in that long injection paths can be avoided and parasitic pumping of Bragg reflectors can be eliminated. In fact, the very first electrically pumped quasi-cw room-temperature operation of an RPG laser was recently achieved by using the transverse-junction approach [Schaus 1991].

While a strained-quantum-well active region is attractive for microlasers, incorporation of strained-layer materials in the RPG structures [Gourley 1989b] still represents a significant technological challenge. Due to multiplicity of active layers their cumulative thickness may easily exceed the critical thickness for dislocation-free accommodation of strain, leading to a metastable configuration.

7. THERMAL EFFECTS

Excessive heating of surface-emitting lasers represents a major impediment preventing further increase of their output power and development of densely-packed two-dimensional arrays. Thermal power densities generated inside the active region of VC-SELs are extremely high [Nakwaski 1991b]. This leads to a substantial increase of temperature and a corresponding increase in the threshold current density. The fact that the first room-temperature cw operation of VC-SELs was only reported two years ago [Ibaraki 1989], [Koyama 1989b] is mainly due to difficulties with overcoming the heating problems. The active-region temperature of the VC-SELs at threshold of cw operation has been estimated to be 25-30 °C higher than that of the substrate [Tai 1989b]. In contrast, the active-region heating near threshold in edge-emitting stripe lasers does not typically exceed 2-5 °C [Duda 1979], [Yano 1981], [Ito 1981], [Manning 1981]. Efficient heat dissipation, along with ultra-low threshold, is therefore critical for applications requiring massive integration. In addition, since the operating lifetime of the device decreases exponentially with temperature, it is essential to design lasers with consistently low self-heating.

Thermal problems will be even more pressing in arrays of VC-SELs, where long-range thermal cross-talk will have to be avoided. As the technology of surface-emitting lasers matures, optimization of their thermal properties will represent a major task to be solved in order to meet the requirements of massive integration necessary for optical processing applications.

In spite of their importance for individual device performance, large-scale integration ca-

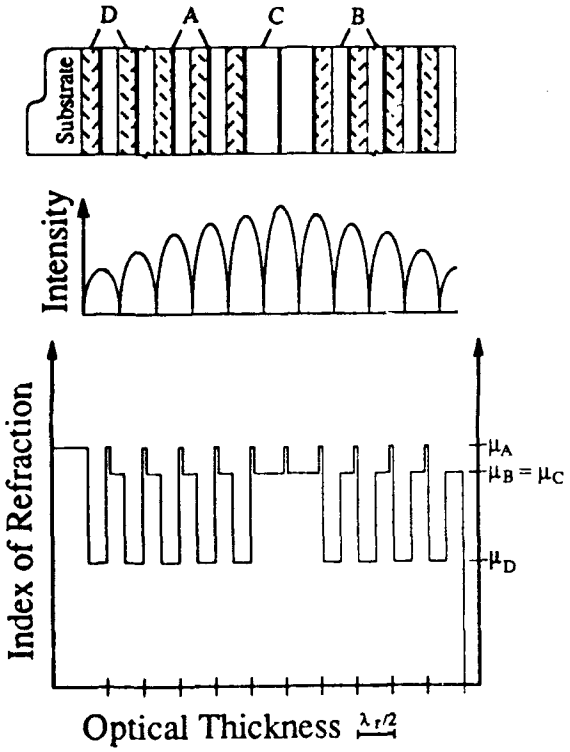

Fig. 7. Schematic illustration of layer structure, optical intensity distribution, and refractive index profile in a DFB-RPG analogue of microlaser. Layer designation is the same as in Fig. 2.

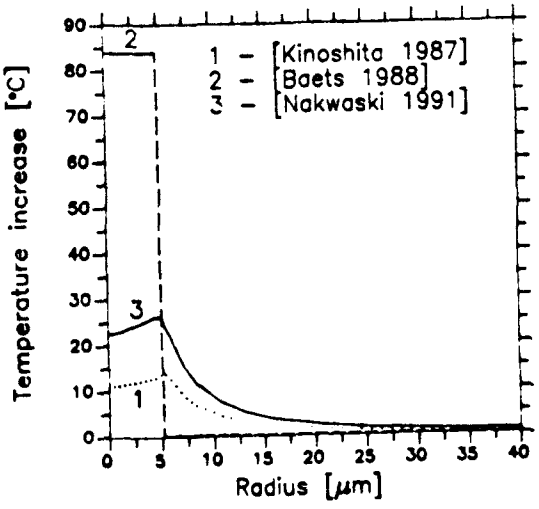

Fig. 8. Temperature profiles in an etched-well DH VC-SEL with 5-μm radius, calculated using various thermal models. The pumping current I = 30 mA $\simeq 2I_{th}$.

pabilities, and device reliability, thermal effects in VC-SELs received very little attention so far. The complexity of thermal problems in VC-SELs may be at least partially responsible for this. In contrast to edge-emitting diode lasers, where nonradiative recombination of charge carriers in the active region is a strongly dominant heat source, surface-emitting lasers have a much more complicated distribution of heat sources. In addition, analytical description of heat flux spreading in a cylindrically symmetric structure is more complicated than in a rectangular edge-emitting structure. Consequently, self-consistent solution of the thermal problem in a VC-SEL represents a difficult computational task.

Early attempts to address thermal problems in VC-SELs involved rather crude approximations. Kinoshita *et al.* [Kinoshita 1987] assumed a uniform heat source distribution in the active region and neglected the Joule heating, which in VC-SELs plays a much more important role than in edge emitters. Baets [Baets 1988] treated heat-spreading as one-dimensional, in addition to uniform distribution of heat sources. These deficiencies have been removed in a recent comprehensive treatment of thermal effects in etched-well vertical-cavity surface-emitting lasers, featuring realistic distribution of heat sources and two-dimensional analysis of both current and heat spreading [Nakwaski 1991b]. Fig. 8 illustrates inaccuracies in predicted temperature profiles that arise when unrealistic assumptions are made. Particularly inadequate is the one-dimensional treatment of [Baets 1988], strongly exaggerating thermal problems by neglecting the lateral heat spreading, which in structures of cylindrical symmetry is of critical importance. This results in errors as high as 220% in predicted temperature distribution in the active region [Nakwaski 1991a]. It is also shown in [Nakwaski 1991b] that by simple technological means it is possible to ease severity of heating effects.

Although in principle excessive heating should be avoided, it is worthwhile mentioning that thermal effects in VC-SELs are not always detrimental. In particular, increased temperature in the active region produces thermal waveguiding effect [Nakwaski 1991b] which may be responsible for reduced cw threshold currents in gain-guided proton-implanted microlasers [Lee 1990c]. Pulsed thresholds over two times higher than in cw conditions were reported [Hasnain 1990].

Most VC-SEL structures exhibit increasing threshold current densities when device diameter is reduced below, say, 30 μm. Large diameter lasers experience smaller losses due to diffraction and diffusion, which results in lower thresholds. However, when the diameter is too large, the heating problems become more important, since the heat dissipation becomes essentially one-dimensional. There is, therefore, a trade-off between reducing losses and maintaining efficient heat sinking, which leads to optimal device size.

8. FUTURE PROSPECTS AND CONCLUSIONS

From an energy standpoint, replacing electrical interconnections with optical elements should in general reduce the total operating energy for communications over all but the shortest intrachip distances [Miller 1989]. Small arrays of VC-SELs should therefore be able to accomplish high-speed communication between electronic chips. Arrays of laser-based logic gates may be used for photonic switching in communication networks or for digital or neural computing. In all of these applications, it is essential to minimize the threshold current for lasing operation. To compete successfully against either electronic interconnections or optical modulators, the energy consumed by the laser per bit of transmitted information should compare favorably to energy requirements of the other sources. This translates to thresholds on the order of 100 μA [Jewell 1990a].

The lowest VC-SEL room-temperature cw threshold current reported to date is 0.7 mA for

a 7-μm square microlaser [Geels 1990b]. This compares very well with the lowest threshold in edge-emitting lasers (0.55 mA), achieved by optimizing a GRIN-SCH (graded-index separate confinement heterostructure) structure containing a single quantum well active region [Lau 1988]. Further progress should be possible, and the goal of 100 μA seems to be quite realistic. Improved passivation of sidewalls in columnar microlasers is expected to reduce threshold current in 1-μm diameter devices to less than 10 μA [Jewell 1990b].

The lowest cw threshold current density (800 A/cm^2) [Geels 1990a] reported for microcavity VC-SELs with strained quantum well active regions is still six times higher than the best result obtained in long-cavity edge-emitting structures (120 A/cm^2 [Chen 1990]). In addition, these low values of microlaser threshold current densities have been obtained solely for relatively broad-area emitters (~150 μm^2), while rapid increase of threshold was observed for small-area (<100 μm^2) devices. Further improvement in reducing the threshold current density will require very good quality of DBR mirrors with reflectivities exceeding 99% combined with suppressed nonradiative surface recombination in columnar microlasers or minimized current spreading in planar structures.

The microlaser structure, in which the active region coincides with an antinode of the lasing mode, has the advantage of very low threshold at the expense of small output power. On the other hand, resonant-periodic-gain (RPG) VC-SELs with multiple active regions offer impressively high output powers and high efficiencies. Consequently, the RPG devices represent a promising source for high-performance parallel networks with large numbers of processing elements, where the optical power requirements become more stringent. Another attractive area of applications for high-power VC-SELs is optical recording.

Possibility of photonic bandgaps in structures with three-dimensional periodicity [Yablonovitch 1987] represents a major attraction for VC-SELs since it implies effective inhibition of undesirable spontaneous emission. However, theoretical understanding of photonic bandgaps needs to be improved before such concept could be seriously entertained for semiconductor lasers. It has been recently shown [Leung 1990], [Zhang 1990], [Ho 1990b] that when the vector nature of the electromagnetic field is included in the analysis of fcc structures, the gaps obtained in scalar calculations disappear. At this point, it is not yet clear what conditions need to be satisfied in order to obtain the photonics bandgaps.

In summary, vertical-cavity surface-emitting semiconductor lasers are now at the stage of dynamic development. Their architecture is ideal for many novel applications. At a low-power end, such as interchip communication, microresonator VC-SELs with a single quantum well active region are the sources of choice. At a high-power end, corresponding for example to massively parallel interconnects or optical recording, highly-efficient resonant-periodic-gain structures with multiple active regions offer the best prospects. Among the most recent advancements, a novel DFB-RPG structure for vertical-cavity surface-emitting lasers seems particularly promising.

9. ACKNOWLEDGMENTS

The author wishes to thank his students and colleagues at the University of New Mexico, and particularly Mohammad Mahbobzadeh, Steven Kubica, and Drs. Christian Schaus, Włodzimierz Nakwaski, Julian Cheng, and Steven Brueck, for their fine collaboration and assistance during the course of research work on VC-SELs at UNM. Support of the U.S. Air Force Office of Scientific Research, the Phillips Laboratory, and the Defense Advanced Research Projects Agency is gratefully acknowledged.

10. REFERENCES

[Baets 1988] R. Baets, "Considerations on Geometry Design of Surface-Emitting Laser Diodes", *IEE Proc. Pt. J (Optoelectron.)*, vol. 135, pp. 233-241, June 1988.

[Botez 1989] D. Botez, L. M. Zinkiewicz, T. J. Roth, L. J. Mawst, and G. Peterson, "Low-Threshold-Current-Density Vertical-Cavity Surface-Emitting AlGaAs/GaAs Diode Lasers", *IEEE Photon. Technol. Lett.*, vol. 1, pp. 205-208, Aug. 1989.

[Chang-Hasnain 1990a] C. J. Chang-Hasnain, M. Orenstein, A. Von Lehmen, L. T. Florez, J. P. Harbison, and N. G. Stoffel, "Transverse Mode Characteristics of Vertical Cavity Surface-Emitting Lasers", *Appl. Phys. Lett.*, vol. 57, pp. 218-220, 16 July 1990.

[Chang-Hasnain 1990b] C. J. Chang-Hasnain, M. W. Maeda, N. G. Stoffel, J. P. Harbison, L. T. Florez, and J. Jewell, "Surface-Emitting Laser Arrays with Uniformly Separated Wavelengths", *Electron. Lett.*, vol. 26, pp. 940-942, 21 June 1990.

[Chang-Hasnain 1991] C. J. Chang-Hasnain, J. R. Wullert, J. P. Harbison, L. T. Florez, N. G. Stoffel, and M. W. Maeda, "Rastered, Uniformly Separated Wavelengths Emitted from a Two-Dimensional Vertical-Cavity Surface-Emitting Laser Array", *Appl. Phys. Lett.*, vol. 58, pp. 31-33, 7 Jan. 1991.

[Chen 1990] T. R. Chen, L. Eng, B. Zhao, Y. H. Zhuang, S. Sanders, H. Morkoç, and A. Yariv, "Submilliamp Threshold InGaAs-GaAs Strained Layer Quantum-Well Laser", *IEEE J. Quantum Electron.*, vol. 26, pp. 1183-1190 (1990).

[Clausen 1990] E. M. Clausen, Jr., A. Von Lehmen, C. Chang-Hasnain, J. P. Harbison, and L. T. Florez, "Greatly Improved Threshold Characteristics of Vertical-Cavity Surface-Emitting Lasers Fabricated by a Unique Etching Process", *Techn. Digest Postdeadline Papers, OSA 1990 Annual Meeting*, Boston, MA, Nov. 4-9, 1990, Paper PDP 21, pp. 52-54.

[Corzine 1989a] S. W. Corzine, R. S. Geels, R.-H. Yan, J. W. Scott, L. A. Coldren, and P. L. Gourley, "Efficient, Narrow-Linewidth Distributed-Bragg-Reflector Surface-Emitting Laser with Periodic Gain", *IEEE Photon. Techn. Lett.*, vol. 1, pp. 52-54, March 1989.

[Corzine 1989b] S. W. Corzine, R. S. Geels, J. W. Scott, R.-H. Yan, and L. A. Coldren, "Design of Fabry-Perot Surface-Emitting Lasers with a Periodic Gain Structure", *IEEE J. Quantum Electron.*, vol. 25, pp. 1513-1524, June 1989.

[Deppe 1989] D. G. Deppe, A. Y. Cho, K. F. Huang, R. J. Fischer, K. Tai, E. F. Schubert, and J. F. Chen, "AlGaAs-GaAs and AlGaAs-GaAs-InGaAs Vertical Cavity Surface Emitting Lasers with Ag Mirrors", *J. Appl. Phys.*, vol. 66, pp. 5629-5631, 1 Dec. 1989.

[Deppe 1990] D. G. Deppe, J. P. van der Ziel, N. Chand, G. J. Zydzik, and S. N. G. Chu, "Phase-Coupled Two-Dimensional $Al_xGa_{1-x}As$-GaAs Vertical-Cavity Surface-Emitting Laser Array", *Appl. Phys. Lett.*, vol. 56, pp. 2089-2091, 21 May 1990.

[Duda 1979] E. Duda, J.-C. Carballes, and J. Apruzzese, "Thermal Resistance and Temperature Distribution in Double-Heterostructure Lasers: Calculations and Experimental Results", *IEEE J. Quantum Electron.* vol. QE-15, pp. 812-817, Aug. 1979.

[Feldman 1988] M. R. Feldman, S. C. Esener, C. C. Guest, and S. H. Lee, "Comparison Between Optical and Electrical Interconnects Based on Power and Speed Considerations", *Appl. Opt.*, vol. 27, pp. 1742-1751, 1 May 1988.

[Fischer 1990] R. J. Fischer, K. Tai, M. Hong, J. M. Vanderberg, J. Y. Ying, J. P. Mannaerts, and A. Y. Cho, "Use of Hybrid Reflectors to Achieve Low Thresholds in All Molecular-Beam Epitaxy Grown Vertical Cavity Surface Emitting Laser Diodes", *J. Vac. Sci. Technol. B*, vol. 8, pp. 336-338, March 1990.

[Geels 1988] R. S. Geels, R. H. Yan, J. W. Scott, S. W. Corzine, R. J. Simes, and L. A. Coldren, "Analysis and Design of a Novel Parallel-Driven MQW-DBR Surface-Emitting Diode Laser", *CLEO '88 Conf. Lasers & Electro-Optics. Techn. Digest Series Vol. 7*, Anaheim, CA, April 25-29, 1988, Paper WM1, pp. 206-207.

[Geels 1990a] R. S. Geels and L. A. Coldren, "Low Threshold Planarized Vertical-Cavity Surface-Emitting Lasers", *IEEE Photon. Techn. Lett.*, vol. 2, pp. 234-236, April 1990.

[Geels 1990b] R. S. Geels and L. A. Coldren, "Submilliamp Threshold Vertical-Cavity Laser Diodes", *Appl. Phys. Lett.*, vol. 57, pp. 1605-1607, 15 Oct. 1990.

[Goodman 1984] J. W. Goodman, F. J. Leonberger, S.-Y. Kung, and R. A. Athale, "Optical Interconnections for VLSI Systems", *Proc. IEEE*, vol. 72, pp. 850-866, July 1984.

[Gourley 1987] P. L. Gourley and T. J. Drummond, "Visible, Room-Temperature, Surface-Emitting Laser Using an Epitaxial Fabry-Perot Resonator with AlGaAs/AlAs Quarter-Wave High Reflectors and AlGaAs/GaAs Multiple Quantum Wells", *Appl. Phys. Lett.*, vol. 50, pp. 1225-1227, 4 May 1987.

[Gourley 1989a] P. L. Gourley, T. M. Brennan, B. E. Hammons, S. W. Corzine, R. S. Geels, R. H. Yan, J. W. Scott, and L. A. Coldren, "High-Efficiency TEM_{00} Continuous-Wave (Al,Ga)As Epitaxial Surface-Emitting Lasers and Effect of Half-Wave Periodic Gain", *Appl. Phys. Lett.*, vol. 54, pp. 1209-1211, 27 March 1989.

[Gourley 1989b] P. L. Gourley, S. K. Lyo, and L. R. Dawson, "High-Efficiency, Continuous-Wave, Epitaxial Surface-Emitting Laser with Pseudomorphic InGaAs Quantum Wells", *Appl. Phys. Lett.*, vol. 54, pp. 1397-1399, 10 April 1989.

[Hasnain 1990] G. Hasnain, K. Tai, J. D. Wynn, Y. H. Wang, R. J. Fischer, B. E. Weir, and A. Y. Cho, "High Frequency Modulation and Efficient Fiber Coupling of Vertical Cavity Surface Emitting Lasers", *Post Deadline Papers, LEOS 1990 Annual Meeting*, Boston, MA, Nov. 4-9, 1990, Paper PD11, and *LEOS'90 Conf. Proc.*, pp. 662-663.

[Hillerich 1988] B. Hillerich, "Shape Analysis and Coupling Loss of Microlenses on Single-Mode Fiber Tips", *Appl. Opt.*, vol. 27, pp. 3102-3105, 1 Aug. 1988.

[Ho 1990a] S.-T. Ho, S. L. McCall, R. E. Slusher, L. N. Pfeiffer, K. W. West, A. F. J. Levi, G. E. Blonder, and J. L. Jewell, "High Index Contrast Mirrors for Optical Microcavities", *Appl. Phys. Lett.*, vol. 57, pp. 1387-1389, 1 Oct. 1990.

[Ho 1990b] K. M. Ho, C. T. Chan, and C. M. Soukoulis, "Existence of Photonic Gap in Periodic Dielectric Structures", *Phys. Rev. Lett.*, vol. 65, pp. 3152-3155, 17 Dec. 1990.

[Hsin 1990] W. Hsin, G. Du, J. K. Gamelin, K. J. Malloy, S. Wang, J. R. Whinnery, Y. J. Yang, T. G. Dziura, and S. C. Wang, "Low Threshold Distributed Bragg Reflector Surface Emitting Laser Diode with Semiconductor Air-Bridge-Supported Top Mirror", *Electron. Lett.*, vol. 26, pp. 307-308, 1 March 1990.

[Huang 1989] K. F. Huang, K. Tai, J. L. Jewell, R. J. Fischer, S. L. McCall, and A. Y. Cho, "Room-Temperature Pseudomorphic $In_xGa_{1-x}As/GaAs$ Quantum Well Surface-Emitting Lasers at 0.94-1.0 μm Wavelengths", *Appl. Phys. Lett.*, vol. 54, pp. 2192-2194, 29 May 1989.

[Ibaraki 1989] A. Ibaraki, K. Kawashima, K. Furusawa, T. Ishikawa, T. Yamaguchi, and T. Niina, "Buried Heterostructure GaAs/GaAlAs Distributed Bragg Reflector Surface Emitting Laser with Very Low Threshold (5.2 mA) under Room Temperature CW Conditions", *Jpn. J. Appl. Phys.*, vol. 28, pp. L667-L668, April 1989.

[Iga 1988] K. Iga, F. Koyama, and S. Kinoshita, "Surface Emitting Semiconductor Lasers", *IEEE J. Quantum Electron.*, vol. 24, pp. 1845-1855, Sept. 1988, and the references quoted therein.

[Ito 1981] M. Ito and T. Kimura, "Stationary and Transient Thermal Properties of Semiconductor Laser Diodes", *IEEE J. Quantum Electron.*, vol. QE-17, pp. 787-795, May 1981.

[Jewell 1989a] J. L. Jewell, S. L. McCall, Y. H. Lee, A. Scherer, A. C. Gossard, and J. H. English, "Lasing Characteristics of GaAs Microresonators", *Appl. Phys. Lett.*, vol. 54, pp. 1400-1402, 10 April 1989.

[Jewell 1989b] J. L. Jewell, K. F. Huang, K. Tai, Y. H. Lee, R. J. Fischer, S. L. McCall, and A. Y. Cho, "Vertical Cavity Single Quantum Well Laser", *Appl. Phys. Lett.*, vol. 55, pp. 424-427, 31 July 1989.

[Jewell 1989c] J. L. Jewell, A. Scherer, S. L. McCall, Y. H. Lee, S. Walker, J. P. Harbison, and L. T. Florez, "Low-Threshold Electrically Pumped Vertical-Cavity Surface-Emitting Microlasers", *Electron. Lett.*, vol. 25, pp. 1123-1124, 17 Aug. 1989.

[Jewell 1990a] J. L. Jewell, Y. H. Lee, A. Scherer, S. L. McCall, N. A. Olsson, J. P. Harbison, and L. T. Florez, "Surface-Emitting Microlasers for Photonic Switching and Interchip Connections", *Opt. Eng.*, vol. 29, pp. 210-214, March 1990.

[Jewell 1990b] J. L. Jewell, A. Scherer, Y. H. Lee, S. L. McCall, J. P. Harbison, L. T. Florez, R. S. Tucker, C. A. Burrus, C. J. Sandroff, and N. A. Olsson, "Vertical Cavity Surface Emitting Microlasers", , *LEOS'90 Conf. Proc., LEOS 1990 Annual Meeting*, Boston, MA, Nov. 4-9, 1990, Paper SDL1.2/MKK2, p. 378.

[Kinoshita 1987] S. Kinoshita, F. Koyama, and K. Iga, "Investigation of the CW Operation at Room Temperature for GaAlAs/GaAs Surface Emitting Laser", *Proc. Tech. Group Meet., IECE Japan*, paper OQE86-188, pp. 23-30, 16 March 1987.

[Koyama 1989b] F. Koyama, S. Kinoshita, and K. Iga, "Room-Temperature Continuous Wave Lasing Characteristics of a GaAs Vertical Cavity Surface-Emitting Laser", *Appl. Phys. Lett.*, vol. 55, pp. 221-222, 17 July 1989.

[Lau 1988] K. Y. Lau, P. L. Derry, and A. Yariv, "Ultimate Limit in Low Threshold Quantum Well GaAlAs Semiconductor Lasers", *Appl. Phys. Lett.*, vol. 52, pp. 88-90, 11 Jan. 1988.

[Lee 1989] Y. H. Lee, J. L. Jewell, A. Scherer, S. L. McCall, J. P. Harbison, and L. T. Florez, "Room-Temperature Continuous-Wave Vertical-Cavity Single-Quantum-Well Microlaser Diodes", *Electron. Lett.*, vol. 25, pp. 1377-1378, 28 Sept. 1989.

[Lee 1990a] Y. H. Lee, J. L. Jewell, B. Tell, K. F. Brown-Goebeler, A. Scherer, J. P. Harbison, and L. T. Florez, "Effects of Etch Depth and Ion Implantation on Surface-Emitting Microlasers", *Electron. Lett.*, vol. 26, pp. 225-227, 15 Feb. 1990.

[Lee 1990b] Y. H. Lee, B. Tell, K. Brown-Goebeler, J. L. Jewell, and J. V. Hove, "Top Surface-Emitting GaAs Four-Quantum-Well Lasers Emitting at 0.85 μm", *Electron. Lett.*, vol. 26, pp. 710-711, 24 May 1990.

[Lee 1990c] Y. H. Lee, B. Tell, K. Brown-Goebeler, J. L. Jewell, R. E. Leibenguth, M. T. Asom, G. Livescu, L. Luther, and V. D. Mattera, "High-Efficiency (1.2 mW/mA) Top-Surface-Emitting GaAs Quantum Well Lasers", *Electron. Lett.*, vol. 26, pp. 1308-1310, 2 Aug. 1990.

[Leung 1990] K. M. Leung and Y. F. Liu, "Full Vector Wave Calculation of Photonic Band Structures in Face-Centered-Cubic Dielectric Media", *Phys. Rev. Lett.*, vol. 65, pp. 2646-2649, 19 Nov. 1990.

[Mahbobzadeh 1990] M. Mahbobzadeh and M. Osiński, "Novel Distributed-Feedback Resonant-Periodic-Gain Structure for Vertical-Cavity Surface-Emitting Semiconductor Lasers", *Electron. Lett.*, vol. 26, pp. 1716-1718, 27 Sept. 1990.

[Manning 1981] J. S. Manning, "Thermal Impedance of Diode Lasers: Comparison of Experimental Methods and a Theoretical Model", *J. Appl. Phys.*, vol. 52, pp. 3179-3184, May 1981.

[Miller 1989] D. A. B. Miller, "Optics for Low-Energy Communication Inside Digital Processors: Quantum Detectors, Sources, and Modulators as Efficient Impedance Converters", *Opt. Lett.*, vol. 14, pp. 146-148, 15 Jan. 1989.

[Nakwaski 1991a] W. Nakwaski and M. Osiński, "Temperature Profiles in Etched-Well Surface-Emitting Semiconductor Lasers", *Jpn. J. Appl. Phys.*, vol. 30, 1 April 1991.

[Nakwaski 1991b] W. Nakwaski and M. Osiński, "Thermal Properties of Etched-Well Surface-Emitting Semiconductor Lasers", *IEEE J. Quantum Electron.*, vol. 27, June 1991.

[Ogura 1991] M. Ogura, "Progress of Surface-Emitting Lasers in Japan", this volume.

[Orenstein 1990] M. Orenstein, A. C. Von Lehmen, C. Chang-Hasnain, N. G. Stoffel, J. P. Harbison, L. T. Florez, E. Clausen, and J. E. Jewell, "Vertical-cavity surface-emitting InGaAs/GaAs lasers with planar lateral definition", *Appl. Phys. Lett.*, vol. 56, pp. 2384-2386, 11 June 1990.

[Raja 1988a] M. Y. A. Raja, S. R. J. Brueck, M. Osiński, C. F. Schaus, J. G. McInerney, T. M. Brennan, and B. E. Hammons, "Wavelength-Resonant Enhanced Gain/Absorption Structure for Optoelectronic Devices", *Post Deadline Papers, IQEC '88 XVI Int. Conf. Quantum Electron.*, Tokyo, Japan, July 18-21, 1988, Paper PD-23, pp. 52-53.

[Raja 1988b] M. Y. A. Raja, S. R. J. Brueck, M. Osiński, C. F. Schaus, J. G. McInerney, T. M. Brennan, and B. E. Hammons, "Novel Wavelength-Resonant Optoelectronic Structure and Its Application to Surface-Emitting Semiconductor Lasers", *Electron. Lett.*, vol. 24, pp. 1140-1142, 1 Sept. 1988.

[Raja 1988c] M. Y. A. Raja, S. R. J. Brueck, M. Osiński, C. F. Schaus, J. G. McInerney, T. M. Brennan, and B. E. Hammons, "Surface-Emitting Multiple Quantum Well GaAs/AlGaAs Laser with Wavelength-Resonant Periodic Gain Medium", *Appl. Phys. Lett.*, vol. 53, pp. 1678-1680, 31 Oct. 1988.

[Raja 1989] M. Y. A. Raja, S. R. J. Brueck, M. Osiński, C. F. Schaus, J. G. McInerney, T. M. Brennan, and B. E. Hammons, "Resonant Periodic Gain Surface-Emitting Semiconductor Lasers", *IEEE J. Quantum Electron.*, vol. 25, pp. 1500-1512, June 1989.

[Sakaguchi 1988] T. Sakaguchi, F. Koyama, and K. Iga, "Vertical Cavity Surface-Emitting Laser with an AlGaAs/AlAs Bragg Reflector", *Electron. Lett.*, vol. 24, pp. 928-929, 21 July 1988.

[Schaus 1989] C. F. Schaus, H. E. Schaus, S. Sun, M. Y. A. Raja, and S. R. J. Brueck, "MOCVD Growth of GaAs/AlGaAs Wavelength Resonant Periodic Gain Vertical Cavity Surface-Emitting Laser", *Electron. Lett.*, vol. 25, pp. 538-539, 13 April 1989.

[Schaus 1991] C. F. Schaus, A. Torres, J. Cheng, C. Hains, S. Sun, K. Zheng, and E. Armour, "Transverse-Injection Vertical-Cavity Surface-Emitting Lasers with Resonant Periodic Gain ", to be published in *Appl. Phys. Lett.*, vol. 58, 22 April 1991.

[Scherer 1989] A. Scherer, J. L. Jewell, Y. H. Lee, J. P. Harbison, and L. T. Florez, "Fabrication of Microlasers and Microresonator Optical Switches", *Appl. Phys. Lett.*, vol. 55, pp. 2724-2726, 25 Dec. 1989.

[Schubert 1990] E. F. Schubert, L. W. Tu, R. F. Kopf, G. J. Zydzik, and D. G. Deppe, "Low-Threshold Vertical Cavity Surface-Emitting Lasers with Metallic Reflectors", *Appl. Phys. Lett.*, vol. 57, pp. 117-119, 9 July 1990.

[Tai 1989a] K. Tai, R. J. Fischer, K. W. Wang, S. N. G. Chu, and A. Y. Cho, "Use of Implant Isolation for Fabrication of Vertical Cavity Surface-Emitting Laser Diodes", *Electron. Lett.*, vol. 25, pp. 1644-1645, 23 Nov. 1989.

[Tai 1989b] K. Tai, R. J. Fischer, C. W. Seabury, N. A. Olsson, T.-C. D. Huo, Y. Ota, and A. Y. Cho, "Room-Temperature Continuous-Wave Vertical-Cavity Surface-Emitting GaAs Injection Lasers", *Appl. Phys. Lett.*, vol. 55, pp. 2473-2475, 11 Dec. 1989.

[Tai 1990a] K. Tai, L. Yang, Y. H. Wang, J. D. Wynn, and A. Y. Cho, "Drastic Reduction of Series Resistance in Doped Semiconductor Distributed Bragg Reflectors for Surface-Emitting Lasers", *Appl. Phys. Lett.*, vol. 56, pp. 2496-2498, 18 June 1990.

[Tai 1990b] K. Tai, G. Hasnain, J. D. Wynn, R. J. Fischer, Y. H. Wang, B. Weir, J. Gamelin, and A. Y. Cho, "90% Coupling of Top Surface Emitting GaAs/AlGaAs Quantum Well Laser Output into 8 μm Diameter Core Silica Fibre", *Electron. Lett.*, vol. 26, pp. 1628-1629, 13 Sept. 1990.

[Tell 1990] B. Tell, Y. H. Lee, K. F. Brown-Goebeler, J. L. Jewell, R. E. Leibenguth, M. T. Asom, G. Livescu, L. Luther, and V. D. Mattera, "High-Power CW Vertical-Cavity Top Surface-Emitting GaAs Quantum Well Lasers", *Appl. Phys. Lett.*, vol. 57, pp. 1855-1857, 29 Oct. 1990.

[Tu 1990] L.-W. Tu, E. F. Schubert, R. F. Kopf, G. J. Zydzik, M. Hong, S. N. G. Chu, and J. P. Mannaerts, "Vertical-Cavity Surface-Emitting Lasers with Semitransparent Metallic Mirrors and High Quantum Efficiencies", *Appl. Phys. Lett.*, vol. 57, pp. 2045-2047, 12 Nov. 1990.

[van der Ziel 1990] J. P. van der Ziel, D. G. Deppe, N. Chand, G. J. Zydzik, and S. N. G. Chu, "Characteristics of Single- and Two-Dimensional Phase Coupled Arrays of Vertical Cavity Surface Emitting GaAs-AlGaAs Lasers", *IEEE J. Quantum Electron.*, vol. 26, pp. 1873-1882, Nov. 1990.

[Walker 1990] J. D. Walker, K. Malloy, S. Wang, and J. S. Smith, "Precision AlGaAs Bragg Reflectors Fabricated by Phase-Locked Epitaxy", *Appl. Phys. Lett.*, vol. 56, pp. 2493-2495, 18 June 1990.

[Wang 1990a] Y. H. Wang, K. Tai, J. D. Wynn, M. Hong, R. J. Fischer, J. P. Mannaerts, and A. Y. Cho, "GaAs/AlGaAs Multiple Quantum Well GRIN-SCH Vertical Cavity Surface Emitting Laser Diodes", *IEEE Photon. Techn. Lett.*, vol. 2, pp. 456-458, July 1990.

[Wang 1990b] Y. H. Wang, K. Tai, Y. F. Hsieh, S. N. G. Chu, J. D. Wynn, and A. Y. Cho, "Observation of Reduced Current Thresholds in GaAs/AlGaAs Vertical-Cavity Surface-Emitting Lasers Grown on 4° Off-Orientation (001) GaAs Substrates", *Appl. Phys. Lett.*, vol. 57, pp. 1613-1615, 15 Oct. 1990.

[Weber 1990] J.-P. Weber, K. Malloy, and S. Wang, "Effects of Layer Thickness Variations on Vertical-Cavity Surface-Emitting DBR Semiconductor Lasers", *IEEE Photon. Techn. Lett.*, vol. 2, pp. 162-164, March 1990.

[Yablonovitch 1987] E. Yablonovitch, "Inhibited Spontaneous Emission in Solid-State Physics and Electronics", *Phys. Rev. Lett.*, vol. 58, pp. 2059-2062, 5 18 May 1987.

[Yang 1990] L. Yang, M. C. Wu, K. Tai, T. Tanbun-Ek, and R. A. Logan, "InGaAsP(1.3 μm)/InP Vertical-Cavity Surface-Emitting Laser Grown by Metalorganic Vapor Phase Epitaxy", *Appl. Phys. Lett.*, vol. 56, pp. 889-891, 5 March 1990.

[Yano 1981] M. Yano, H. Imai, K. Hori, and M. Takusagawa, "High Temperature Characteristics of Stripe-Geometry InGaAsP/InP Double-Heterostructure Lasers", *IEEE J. Quantum Electron.*, vol. QE-17, pp. 619-626, May 1981.

[Yoo 1990a] H.-J. Yoo, A. Scherer, J. P. Harbison, L. T. Florez, E. G. Paek, B. P. Van der Gaag, J. R. Hayes, A. Von Lehmen, E. Kapon, and Y.-S. Kwon, "Fabrication of a Two-Dimensional Phased Array of Vertical-Cavity Surface-Emitting Lasers", *Appl. Phys. Lett.*, vol. 56, pp. 1198-1200, 26 March 1990.

[Yoo 1990b] H.-J. Yoo, J. R. Hayes, N. Andreadakis, E. G. Paek, G. K. Chang, J. P. Harbison, L. T. Florez, and Y.-S. Kwon, "Low Series Resistance Vertical-Cavity Front-Surface-Emitting Laser Diode", *Appl. Phys. Lett.*, vol. 56, pp. 1942-1944, 14 May 1990.

[Yoo 1990c] H.-J. Yoo, J. R. Hayes, E. G. Paek, A. Scherer, and Y.-S. Kwon, "Array Mode Analysis of Two-Dimensional Phased Array of Vertical Cavity Surface Emitting Lasers", *IEEE J. Quantum Electron.*, vol. 26, pp. 1039-1051, June 1990.

[Zhang 1990] Z. Zhang and S. Satpathy, "Electromagnetic Wave Propagation in Periodic Structures: Bloch Wave Solution of Maxwell's Equations", *Phys. Rev. Lett.*, vol. 65, pp. 2650-2653, 19 Nov. 1990.

[Zinkiewicz 1989] L. M. Zinkiewicz, T. J. Roth, L. J. Mawst, D. Tran, and D. Botez, "High-Power Vertical-Cavity Surface-Emitting AlGaAs/GaAs Diode Lasers", *Appl. Phys. Lett.*, vol. 54, pp. 1959-1961, 15 May 1989.

Thermal Properties of Etched-Well Surface-Emitting Semiconductor Lasers

Włodzimierz Nakwaski and Marek Osiński, *Senior Member, IEEE*

Abstract—**A new comprehensive two-dimensional model for analysis of thermal effects in etched-well vertical-cavity surface-emitting lasers is presented. Self-consistency between electrical and thermal processes is achieved. Joule heating is shown to play a key role in thermal behavior of these devices. Substantial mismatch between current density and optical field profiles can be remedied by proper doping of top cladding layer. A simple way to control the sign and strength of thermal waveguiding is suggested. Consequences for large-scale two-dimensional integration are indicated.**

I. Introduction

RECENT progress in vertical-cavity surface-emitting semiconductor lasers (VC-SEL's) [1]–[3], and especially the achievement of CW room-temperature operation, brings us closer to a prospect for high-efficiency two-dimensional surface-emitting laser arrays [4], [5]. Due to their unique features combining high power capabilities with narrow, nearly circular beams and single-longitudinal-mode operation, such devices are expected to find a wide range of applications as sources for optical interconnections in highly parallel architectures, image processing, optical pattern recognition, free-space optical communications, medicine, etc.

Thermal problems played a significant role since the very beginnings of semiconductor laser history. Failure of early diode lasers to operate CW at room temperature was associated with excessive device heating caused by high threshold current densities. Development of heterostructure lasers has reduced significantly the threshold, which in turn relaxed the severity of thermal effects in those devices. This, however, was not the case of vertical-cavity surface emitting lasers (VC-SEL's) where, as recently as 1988, the pulsed room-temperature threshold current densities were ~30 times larger than the corresponding CW densities in edge emitting lasers [6]. Extremely strong heating induced by such high current densities was responsible for difficulties in achieving a CW room temperature operation of VC-SEL's with bulk active regions that could not be overcome until very recently [7], [8]. The threshold in these devices remains, however, very high (about 10 kA/cm^2 [9]–[12], compared to less than 1 kA/cm^2 in GaAs–AlGaAs edge emitters with similar bulk active regions), which indicates that thermal effects are still critical.

It should be noted that significantly lower threshold current density (~1 kA/cm^2 [13], [14]) was reported recently for microcavity VC-SEL's with strained quantum well active regions, although it still remains an order of magnitude higher than in corresponding edge-emitting structures (120 A/cm^2 [15]). These low values of microlaser threshold current densities, however, have been obtained solely for relatively broad-area emitters (150–1600 μm^2), while rapid increase of threshold was observed for small-area (< 100 μm^2) devices.

Thermal properties of surface-emitting lasers represent a major obstacle on the way toward development of densely packed two-dimensional arrays. Thermal power densities generated inside the active region are extremely high [16], [17]. This leads to a substantial increase of temperature and a corresponding increase in the threshold current density. The active-region temperature of the VC-SEL's at threshold of CW operation has been estimated to be 25–30°C higher than that of the substrate [18]. In contrast, in edge-emitting stripe lasers, the active-region heating near threshold typically does not exceed 2–5°C [19]–[22]. Efficient heat dissipation, along with ultralow threshold, is therefore critical for applications requiring massive integration. In addition, since the operating lifetime of the device decreases exponentially with temperature, it is essential to design lasers with consistently low self-heating. These problems will be even more pressing in arrays of VC-SEL's, and should be addressed early enough to avoid a bottleneck in their development.

In spite of their importance for individual device performance, large-scale integration capabilities and device reliability, thermal effects in VC-SEL's have received very little attention so far. The complexity of thermal problems in VC-SEL's may be at least partially responsible for this. In contrast to edge-emitting diode lasers, where nonradiative recombination of charge carriers in the active region is a strongly dominant heat source, surface-emitting lasers have a much more complicated distribution of heat sources. In addition, analytical description of

Manuscript received November 1, 1990; revised January 31, 1991. The work of W. Nakwaski was supported by the International Research and Exchanges Board (IREX). This work was supported in part by the Defense Advanced Research Projects Agency.

W. Nakwaski is with the Institute of Physics, Technical University of Łódź, Wólczańska 219, 93005 Łódź, Poland, on leave at the Center for High Technology Materials, University of New Mexico, Albuquerque, NM 87131.

M. Osiński is with the Center for High Technology Materials, the Department of Electrical and Computer Engineering, and the Department of Physics and Astronomy, University of New Mexico, Albuquerque, NM 87131.

IEEE Log Number 9100615.

heat flux spreading in a cylindrically symmetric structure is more complicated than in a planar structure. To the best of our knowledge, so far only two attempts to consider thermal properties of single-device VC-SEL's have been made [16], [23]. As demonstrated in Section IV, these models lead to considerable errors in predicted temperature distribution in the device.

In this paper, we formulate a comprehensive thermal model of a VC-SEL which accounts for two-dimensional current and heat spreading, and apply it to analyze a typical ring-contact etched-well structure. The following heat sources are included: nonradiative recombination and reabsorption of spontaneous emission in the active region, Joule heating in cladding layers, and contact heating. Temperature dependence of thermal conductivity, internal efficiencies of spontaneous and stimulated radiative recombination, and threshold current is accounted for self-consistently by an iterative approach.

In the following, a general description of the thermal model of VC-SEL's is presented in Section II. Brief comparison to earlier thermal models of VC-SEL's is given, and their inaccuracy is demonstrated. Details of the model specific to the structure under consideration are discussed in Section III. Section IV contains results of numerical calculations and their discussion. Dominant heat sources are identified, problems with overlap between the optical field and gain profiles are signaled, and strong thermal antiguiding is predicted. Simple technological solutions to overcome these difficulties are suggested. The importance of thermal effects for two-dimensional densely packed arrays is demonstrated.

II. Thermal Model of VC-SEL's—General Description

The basic thermal model of VC-SEL's is composed of three parts: an analytical description of two-dimensional current spreading phenomenon which determines the distribution of heat sources, an equivalent electrical circuit modeling of two-dimensional heat-flux spreading, and calculation of the temperature profiles. Since a nonuniform thermal profile affects material and device parameters used in the current- and heat-spreading calculations, the whole process described above has to be repeated until self-consistency is reached. The self-consistent thermal-electrical solution can only be obtained numerically.

Fig. 1 illustrates the flow chart of calculations leading to both nonself-consistent and self-consistent solutions. The self-consistency criterion consists in requiring that the temperature profiles obtained in two consecutive loops be matched within a prescribed accuracy (better than 1%). in the calculations, we take into account the temperature dependence of the following parameters: thermal conductivities, diode parameter β, threshold current, and internal efficiencies (see Section III).

A. Current Spreading

Current spreading analysis is of primary significance for description of thermal phenomena in VC-SEL's, since

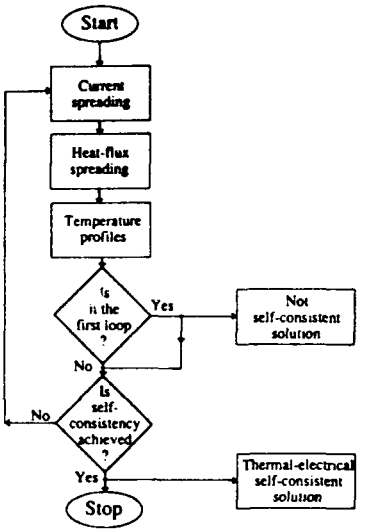

Fig. 1. Flow chart of calculations.

it is directly related to both Joule and active layer heating. Earlier thermal models of VC-SEL's [16], [23] completely neglected any inhomogeneities in current or carrier distributions. In this work, two-dimensional current spreading will be considered. It will be shown in Section IV that the current density does indeed vary significantly within the active region, which confirms that at least for etched-well VC-SEL's, homogeneous distribution of current and heat sources is not a good approximation.

The analysis of current spreading evidently depends on details of a particular device structure, and will therefore be discussed more thoroughly in Section III.

B. Heat Source Distribution

Distribution of heat sources in VC-SEL's is considerably more complicated than in edge-emitting lasers. In the latter case, the nonradiative recombination in the active region is a dominant heat source, and all other sources present in the device can be omitted (see, e.g., [24]). As shown in Section IV, the relative importance of various heat sources in VC-SEL's strongly depends on the pumping current.

Further details regarding distribution of heat sources in a particular device structure will be given in Section III.

C. Heat Flux Spreading and Temperature Profiles

The heat flux spreading is analyzed using an analogy between electrical and thermal phenomena. The structure is transformed into a network of elementary resistors, and the heat generation processes are replaced by elementary current sources. Standard methods of the electrical circuits theory can then be applied, as discussed in more detail in Section III.

For a given distribution of heat sources, the temperature profiles are found using the Green function method. Temperature dependence of thermal conductivity is taken

TABLE I
COMPARISON TO PREVIOUS MODELS OF VC-SEL's

	Kinoshita *et al.* [23]	Baets [16]	This Work
Current spreading	ignored	ignored	considered
Nonradiative recombination	uniform	uniform	nonuniform
Joule heating	ignored	uniform	nonuniform
Heat spreading	2-D	1-D	2-D
Temperature-dependent thermal conductivity	ignored	ignored	considered
Electrical-thermal self-consistency	ignored	ignored	considered

into account in a relatively simple manner by applying the Kirchhoff transformation.

D. Comparison to Previous Thermal Models of VC-SEL's

Major differences between the present model and those used earlier to describe thermal properties of VC-SEL's [16], [23] are highlighted in Table I.

Both previous models completely ignore the two-dimensional (2-D) current-spreading phenomenon, and consequently the heat sources within the active region and within the adjacent passive layers have uniform radial distribution. Our results (see Section IV) indicate that the heat flux density may vary considerably between the center and the edges of the active region, demonstrating that the assumption of uniform current flow is too crude. In addition, Baets [16] applied an oversimplified one-dimensional (1-D) approach to the heat-spreading phenomenon.

Kinoshita *et al.* [23] underestimate the Joule heating, even though, as shown in Section IV, its relative importance is comparable to (and often greater than) that of the active region heating. Baets [16] does consider the Joule heating, however, his assumption of its uniform distribution is even less accurate than in the case of active region heating.

Both earlier models also ignore the temperature dependence of thermal conductivity and do not attempt to achieve any self-consistency between electrical and thermal distributions.

We will show in Section IV that the approximations made in earlier models lead to either a significant underestimate [23] or overestimate [16] of the active-region temperature increase.

III. THERMAL MODEL OF ETCHED-WELL VC-SEL's

Virtually all of the phenomena discussed in Section II—such as the current spreading, distribution of heat sources, and heat flux spreading—strongly depend on structural details of the device. Therefore, before proceeding any further with a description of the thermal model, we need to specify the VC-SEL structure to be considered. Since previous thermal models [16], [23] dealt with etched-well circular VC-SEL's, we will focus our attention on a similar structure shown in Fig. 2, corresponding to a VC-SEL for which successful room-temperature CW operation was reported [7]. This choice will facilitate comparison to the earlier thermal models of VC-SEL's.

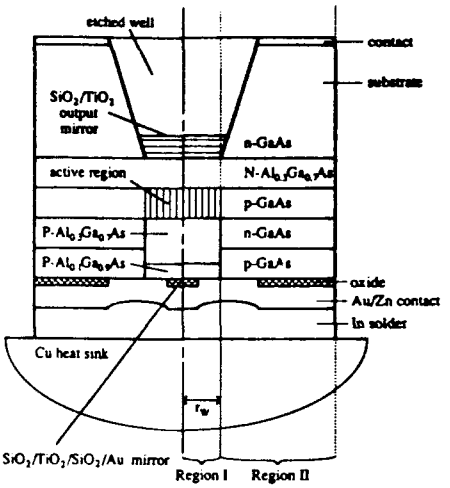

Fig. 2. Schematic structure of an etched-well ring-electrode VC-SEL mounted p-side down.

A. Current Spreading

The most significant current spreading in the ring-contact etched-well VC-SEL structure of Fig. 2 takes place between the substrate and the active region. In the analysis of this process, we will assume the following:

1) the n-GaAs–N-$Al_{0.3}Ga_{0.7}As$ interface is equipotential;

2) the radial current component in the N-$Al_{0.3}Ga_{0.7}As$ layer is neglected for $r > r_w$, where r_w is the radius of etched well;

3) the radial current component in the active region ($r < r_w$) is neglected; and

4) the active region–P-$Al_{0.3}Ga_{0.7}As$ interface is equipotential.

With these assumptions, the current continuity and Ohm's law lead to the following equations:

a) region I ($r < r_w$)

$$\frac{dI_{rn}(r)}{dr} = 2\pi r j_{pn}(r) \tag{1}$$

$$\frac{dU(r)}{dr} = \frac{I_{rn}(r)}{2\pi r} R_n^{(2)} \tag{2}$$

b) region II ($r > r_w$)

$$-\frac{dI_{rp}(r)}{dr} = 2\pi r j_{pn}(r) \tag{3}$$

$$-\frac{dU(r)}{dr} = \frac{I_{rp}(r)}{2\pi r} R_p^{(2)} \tag{4}$$

where I_{rn}, I_{rp}, $R_n^{(2)}$, and $R_p^{(2)}$ stand for radial current components and sheet resistances in the N-$Al_{0.3}Ga_{0.7}As$ cladding layer and in the passive p-GaAs region adjacent to

the active region, respectively. j_{pn} is the current density through the p-GaAs-N-$Al_{0.3}Ga_{0.7}As$ interface, which is related to the voltage drop U at the p–N junction by the well-known equation

$$j_{pn}(r) = j_0 \exp[\beta U(r)], \tag{5}$$

where j_0 is the reverse saturation current density and

$$\beta = \frac{e}{mk_BT}. \tag{6}$$

Here e is the electron charge, k_B is the Boltzmann constant, and m is a quality factor ($m \simeq 2$ for GaAs-AlGaAs junctions [25]).

Equations (1)-(4) have to be complemented by boundary conditions

$$I_{rn}(0) = 0, \tag{7}$$

$$I_{rp}(\infty) = 0. \tag{8}$$

The problem described by (1)-(8) has been solved analytically by Bugajski and Kontkiewicz [26], with the solution given by

$$j_{pn}(r) = \begin{cases} \dfrac{I_{Bn}r_w^2(1 + I_{Bn}/I_A)}{\pi[r_w^2(1 + I_{Bn}/I_A) - r^2]^2}, & \text{for } r \le r_w \\ \dfrac{I_{Bp}r_w^2[1 - I_{Bp}/(I_T - I_A)]}{\pi\{r^2 - r_w^2[1 - I_{Bp}/(I_T - I_A)]\}^2} & \\ & \text{for } r \ge r_w \end{cases} \tag{9}$$

$$U(r) = \begin{cases} U_A + \dfrac{2}{\beta}\ln\dfrac{r_w^2(I_{Bn}/I_A)}{r_w^2(1 + I_{Bn}/I_A) - r^2} & \\ & \text{for } r \le r_w \\ \dfrac{1}{\beta}\ln\dfrac{r_w^2 I_{Bp}|1 - I_{Bp}/(I_T - I_A)|}{j_0\pi\{r^2 - r_w^2[1 - I_{Bp}/(I_T - I_A)]\}^2} & \\ & \text{for } r \ge r_w \end{cases} \tag{10}$$

with

$$I_{Bn} = \frac{8\pi}{\beta R_n^{(2)}} \tag{11}$$

$$I_{Bp} = \frac{8\pi}{\beta R_p^{(2)}} \tag{12}$$

$$I_A = \frac{R_p^{(2)}I_T}{R_p^{(2)} - R_n^{(2)}} - \left[\frac{8\pi I_T(R_p^{(2)} - R_n^{(2)}) + \beta R_p^{(2)}R_n^{(2)}I_T^2}{\beta(R_p^{(2)} - R_n^{(2)})^2}\right]^{1/2} \tag{13}$$

$$U_A = \frac{1}{\beta}\ln\frac{I_A(1 + I_A/I_{Bn})}{j_0\pi r_w^2} \tag{14}$$

where I_T stands for the total pumping current.

The current density $j_p(r)$ flowing through the P-$Al_{0.3}Ga_{0.7}As$ layer is approximated to have the same radial profile as $j_{pn}(r)$. The p-contact current density is assumed to change as $1/r$.

B. Heat Source Distribution

Distribution of the major heat sources within an etched-well VC-SEL structure is schematically shown in Fig. 3.

The active region heating, by far the most important heat source in edge-emitting lasers, remains one of the dominant thermal processes in VC-SEL's. Neglecting any nonuniformities along the z direction, the heat density distribution can be obtained by considering nonradiative recombination and absorption of spontaneous radiation in the active region [27], which leads to

$$g_a = \frac{U(r)(1 - \eta_{sp}f_{sp})}{d} \cdot \{j_{th}(T) + [j_{pn}(r) - j_{th}(T)](1 - \eta_i)\} \quad [\mathrm{W/cm^3}] \tag{15}$$

where η_{sp} and η_i are internal quantum efficiencies of spontaneous and stimulated emission, respectively, f_{sp} is a factor accounting for escape of spontaneous light from the active region [28], and $j_{th}(T)$ is an adjusted threshold current density which takes into account an increase of temperature inside the active region. The threshold current density is assumed to constitute a constant fraction of the total current density in the whole active region. The temperature dependence of the threshold is described by the familiar Arrhenius-type relation:

$$j_{th}(T) = j_{th}(300)\exp[(T - 300)/T_0], \tag{16}$$

with temperature expressed in Kelvin. Note that $j_{th}(300)$ corresponds to threshold in a laser whose active region temperature is 300 K, which is equivalent to room-temperature pulsed threshold.

The temperature dependence of η_{sp} and η_i is assumed to obey a relation similar to that given in [29] for the differential quantum efficiency:

$$\eta_{sp(i)}(T) = \eta_{sp(i)}(300)\exp[-(T - 300)/2T_0]. \tag{17}$$

The main sources of Joule heating are in both confinement layers and in the p-contact region. For the confinement layers, the corresponding heat density can be expressed as

$$g_{N(P)}(r) = j_{N(P)}^2(r)\rho_{N(P)}, \tag{18}$$

with $\rho_{N(P)}$ standing for the electrical resistivity (in Ωcm) of the $N(P)$-confinement layer.

A similar formula is used to find the heat-flux density generated in the p-contact region:

$$q_c(r) = j_c^2(r)\rho_c, \quad [\mathrm{W/cm^2}] \tag{19}$$

where ρ_c is the contact resistivity (in $\Omega\mathrm{cm}^2$).

C. Heat Flux Spreading

In order to analyze the heat flux spreading, we construct an electrical equivalent of the structure which can

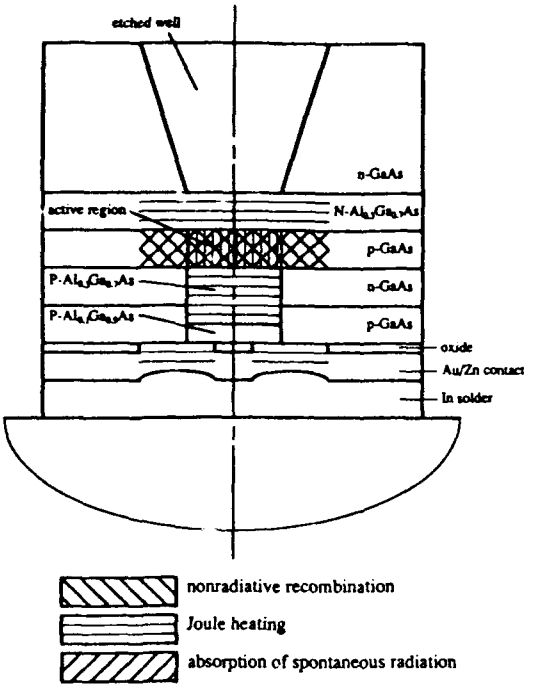

Fig. 3. Schematic diagram indicating distribution of major heat sources in etched-well VC-SEL.

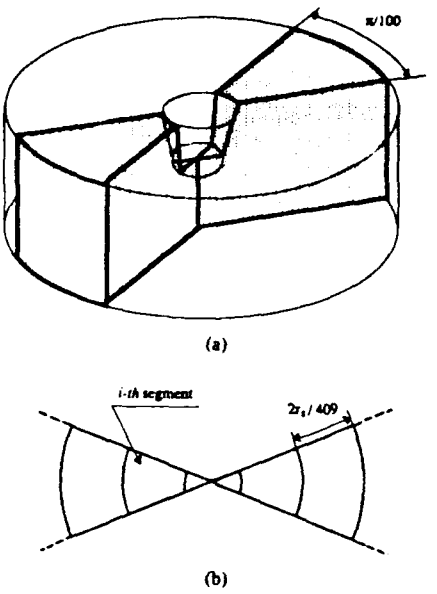

Fig. 4. Schematic of the procedure of dividing (a) the entire structure into cylindrically symmetric bowtie elements, and (b) a single bowtie element into small segments.

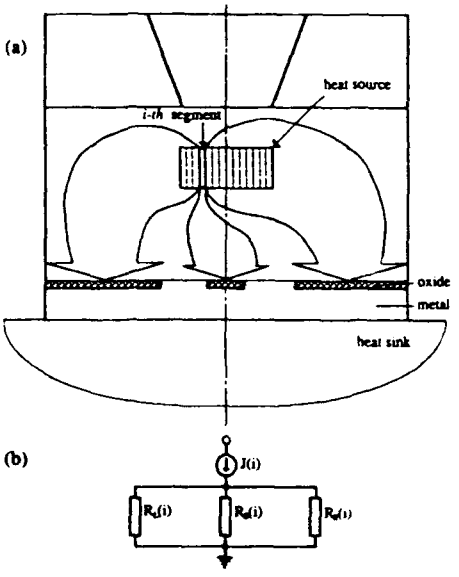

Fig. 5. (a) Schematic heat flux spreading from a single segment shown in Fig. 4(b), and (b) corresponding simple equivalent electrical circuit.

be solved using standard circuit theory. The cylindrical symmetry of etched-well VC-SEL permits to simplify the problem by dividing the entire device into a large number (100) of bowtie prisms, each consisting of two diametrically opposite elements [see Fig. 4(a)], and considering only one such prism with periodic boundary conditions. Each prism is then further divided into a large number (409) of segments [Fig. 4(b)], and the spreading of heat generated in each segment is considered using an equivalent electrical circuit shown schematically in Fig. 5. All electrical resistances in Fig. 5(b) are in fact chains of many elementary resistances extending over the whole structure. Contributions to heat flux spreading from each segment are considered separately, with final results obtained via a superposition rule. The method is described in more detail in [30].

While the heat flux spreading in semiconducting part of the structure is truly two dimensional, we can expect that the heat flow through the oxide and contact/solder layers will be one dimensional. This is due to the fact that the thermal conductivity of the oxide layers is very low, the contact layer is very thin, and the thermal conductivity of In solder is several times lower than that of the Cu heat sink.

D. Temperature Profiles

Consider first the temperature profiles in the semiconducting part of the structure in which the heat flow is two dimensional. Analytical solution of the thermal conduction equation is available for a homogeneous cylindrically symmetrical structure [31], provided that no radial heat transfer takes place at the boundaries of the region under consideration.

Obviously, the etched-well VC-SEL is not a homogeneous structure since it contains layers of different materials. Nevertheless, for the purpose of obtaining the temperature profile in the active region and in the adjacent passive p-GaAs layer, we can replace various materials with thermally equivalent layers of the prevailing material. The semiconducting part of the structure shown in Fig. 2 clearly can be divided in two regions with different prevalent materials: region I ($r < r_w$) which, with the ex-

ceptic n of GaAs active layer, is composed of AlGaAs layers, and region II ($r > r_w$) which, with the exception of N-$Al_{0.3}Ga_{0.7}As$ layer, is composed of GaAs layers. Note that these regions coincide with those introduced in the analysis of current spreading. Hence we replace region I with an equivalent cylinder composed of $Al_{0.3}Ga_{0.7}As$, and we replace region II with a hollow cylinder composed of GaAs. Each layer composed of nonprevalent material is transformed into an equivalent layer of prevalent material simply by multiplying its thickness by a ratio of thermal conductivities of the prevalent material and the transformed layer.

The second requirement for the analytical solution of [31] to be applicable is a boundary condition of no net heat transfer between regions I and II. This is achieved by using the heat flux spreading results of Section III-C. The yield of each segment is modified by adding (or subtracting) contributions arriving from (or entering into) the other region. This leads to a modified distribution of heat sources which allows to treat the heat flow problems in regions I and II separately.

The temperature increase in oxide and solder layers is calculated using the basic formula

$$\Delta T_i = q_{HS} d_i / k_{ci} \tag{20}$$

where d_i and k_{ci} stand for the thickness and thermal conductivity of layer i, and q_{HS} is a heat flux density entering the heat sink. Finally, the temperature profile at the heat sink/solder interface in the region of diameter r_o, where r_o is the outer radius of the ring contact, is obtained by modifying the well-known formula derived for a homogeneous heat source and three-dimensional heat spreading into a semiinfinite medium [32]

$$\Delta T_{HS}(r) = 8 r_o q_{HS}(r) / 3\pi k_{HS} \tag{21}$$

where k_{HS} is the heat sink thermal conductivity.

IV. Discussion of Results

The device parameters assumed in the calculations are given in Table II. The value of f_{sp} is calculated using formulas given in [28]. The SiO_2 and TiO_2 layer thicknesses are taken from [33]. The values of doping concentrations are found in [34]. Electrical resistivities of P- and N-AlGaAs are calculated from measured mobility data given in [35], [36]. The value of p-contact resistance is chosen according to [37]. Thermal conductivities of metal and oxide layers can be found in [38] and [39], respectively. The T_0 value for etched-well VC-SEL's is given in [1]. The remaining parameters are taken from [7] and [40].

Thermal conductivities of $Al_xGa_{1-x}As$ and GaAs layers are obtained from the following relation [41]:

$$k_c(x) = 0.44/(1 + 12.70x - 13.22x^2), \quad \text{W/cm K.} \tag{22}$$

The temperature dependence of k_c determined for GaAs [42] is assumed to be valid for any composition of ternary $Al_xGa_{1-x}As$ [43]:

$$k_c(x, T) = k_c(x, 300\ \text{K})\,(300/T)^{5/4}. \tag{23}$$

TABLE II
Device Parameters for an Etched-Well GaAs-AlGaAs VC-SEL

Parameter	Notation	Value
Pulsed threshold current	I_{th}	15 mA
Internal quantum efficiencies for:		
• lasing	η_i	0.9
• spontaneous emission	η_{sp}	0.5
Spontaneous radiation escape factor	f_{sp}	0.667
Layer thicknesses		
• active	d	2.5 μm
• N-$Al_{0.3}Ga_{0.7}As$	d_N	2.0 μm
• P-$Al_{0.3}Ga_{0.7}As$	d_P	0.9 μm
• P-$Al_{0.1}Ga_{0.9}As$	d_p	0.1 μm
• p-GaAs blocking	d_{pB}	0.3 μm
• n-GaAs blocking	d_{nB}	0.7 μm
• SiO_2	d_{OX1}	301.4 nm
• TiO_2	d_{OX2}	88 nm
• solder	d_s	2.0 μm
Radius of the etched well	r_w	5.0 μm
Inner radius of the bottom contact	r_i	2.5 μm
Outer radius of the bottom contact	r_o	20 μm
Radius of the structure	r_S	50 μm
Thermal conductivities:		
• SiO_2	k_{OX1}	1.38 W/mK
• TiO_2	k_{OX2}	8.4 W/mK
• In	k_s	87 W/mK
• Cu	k_{HS}	401 W/mK
Resistivities		
• N-$Al_{0.3}Ga_{0.7}As$ (N = 7.10^{17} cm^{-3})	ρ_N	$8.5 \cdot 10^{-3}$ Ωcm
• P-$Al_{0.3}Ga_{0.7}As$ (P = 7.10^{17} cm^{-3})	ρ_P	0.135 Ωcm
• p-GaAs (active) (p = 10^{17} cm^{-3})	ρ_p	0.27 Ωcm
Contact resistivity	ρ_C	$1 \cdot 10^{-5}$ Ωcm^2
Reverse saturation current density	j_o	$6 \cdot 10^{-9}$ A/cm^2
Characteristic temperature	T_0	150 K

The room temperature threshold current given in Table II was chosen on the basis of theoretical results of [1], [9], and [16]. For the active region thickness $d = 2.5$ μm and the resonator mirror reflectivities R_1, R_2, such that $R_1 R_2 = 0.95$, the threshold current density should be in the range 15–20 kA/cm^2, which for the active region of radius $r_w = 5$ μm gives $I_{th} = 12$–16 mA.

Unless otherwise stated, the results discussed below correspond to a pumping current of 30 mA.

A. Current Spreading

The importance of a self-consistent approach to thermal-electrical phenomena can already be appreciated by examining Fig. 6, where solid lines represent self-consistent solutions, and dotted lines correspond to nonself-consistent solutions. While very little difference is observed in the current density distributions, the self-consistent solution predicts significantly higher voltage drop, which means that the nonself-consistent solution is expected to underestimate the active region heating. It should be noted that within the active region, the current density changes by a factor of 2.5, thus confirming our assertion that nonuniform junction current injection should be considered.

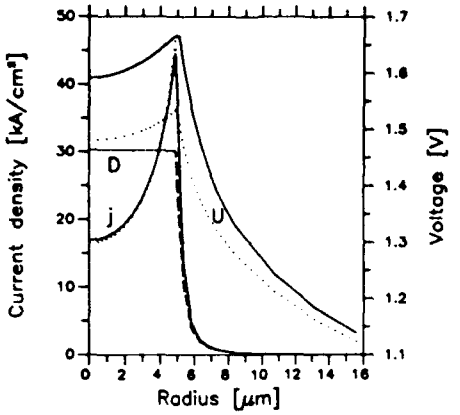

Fig. 6. Distributions of the current density $j_{pn}(r)$ (labeled j) and the voltage drop $U(r)$ at the p–n junction (labeled U). Solid lines represent the thermal-electrical self-consistent solution obtained in 10 iteration loops, while the dotted lines correspond to the nonself-consistent solution. Dashed line labeled D corresponds to a solution obtained by using the approach of [44].

Recently, an analysis of current spreading in VC-SEL's was published [44]. However, as illustrated in Fig. 6, it is considerably less accurate than our approach. The treatment of [44] limits the current spreading considerations only to our region II, outside the active region. It neglects the radial current component in the N-AlGaAs layer, and results in a uniform current injection into the active region. We note that such solution can be easily obtained from (9)–(14) if $R_n^{(2)}$ is set equal to zero.

It should be noted that the current density distribution obtained in self-consistent treatment indicates that the etched-well VC-SEL structure may suffer from poor matching between the optical field of fundamental transverse mode, which has an intensity peak at $r = 0$, and the optical gain, which will have a maximum at the edges of the active region. For this reason, it is important to examine how the inhomogeneity of current density can be reduced.

With the purpose of identifying the key mechanism responsible for inhomogeneity of current density, we examine influence of doping levels in the N-AlGaAs and p-GaAs layers on the current injected into the active region. Fig. 7 shows calculated distributions of the junction carrier density for various doping levels in the above layers. A very important and favorable effect of increasing the donor concentration in the N-AlGaAs layer [Fig. 7(a)] is the improvement in uniformity of injected current density. This is due to reduction of N-AlGaAs sheet resistance which results in deeper penetration of carriers toward the center of the device. In the limit of zero sheet resistance (curve 4), a perfectly uniform distribution would be obtained for the entire active region. On the other hand, increasing the doping level in the p-GaAs layer [Fig. 7(b)] leads to an undesirable behavior, where the current density injected into the active region drops. The improved uniformity in this case is then taking place at a level too low for the lasing action to occur.

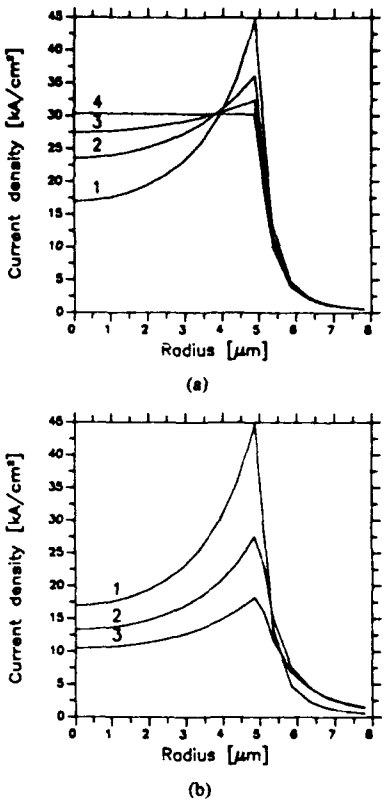

Fig. 7. Dependence of the distribution of the junction current density $j_{pn}(r)$ on doping levels in adjacent passive layers. (a) N-$Al_{0.3}Ga_{0.7}As$ layer concentration of 7×10^{17} cm^{-3} (curve 1), 2×10^{18} cm^{-3} (curve 2), and 7×10^{18} cm^{-3} (curve 3). Curve 4 corresponds to a limit of zero sheet resistance in this layer; (b) p-GaAs layer concentration of 10^{17} cm^{-3} (curve 1), 5×10^{17} cm^{-3} (curve 2), and 10^{18} cm^{-3} (curve 3).

B. Heat Source Distribution

A major difference between this work and earlier studies of VC-SEL thermal properties [16], [23] is that we do not assume uniform heat source distribution. Table III compares heat generation densities due to various heat sources evaluated at three points: in the center, at $r = \frac{1}{2} r_w$, and at $r = r_w$. It is clear that individual heat source yields are strongly inhomogeneous, with the largest variation occurring in the N-AlGaAs layer. It should also be noted that none of the three main heat sources dominates over the others, which distinguishes the VC-SEL structure from edge-emitting lasers in which the active region heating is the only heat source that needs to be considered [24].

Fig. 8 shows pumping current dependence of the total generated power due to various heat sources, obtained by integrating local yields over the entire layer (note that the Joule power generated in the P-AlGaAs layer involves integration from $r = 0$ to $r = r_w$, while the remaining total yields are obtained by extending integration to $r = r_s$). It can be seen that the active region heating dominates at relatively small values of current, while Joule heating in the P-AlGaAs layer becomes the single most important heat source at large values of current. This is due to ap-

TABLE III
SPATIAL VARIATION OF HEAT GENERATION DENSITIES (in W/cm³) ASSOCIATED WITH INDIVIDUAL HEAT SOURCES

Position	Active	P-Layer	N-Layer	Contact
$r = 0$	122.5	62.7	5.2	—
$r = 2.5\ \mu m$	152.2	94.4	21.4	11.6
$r = 5\ \mu m$	338.4	436.4	110.5	3.0

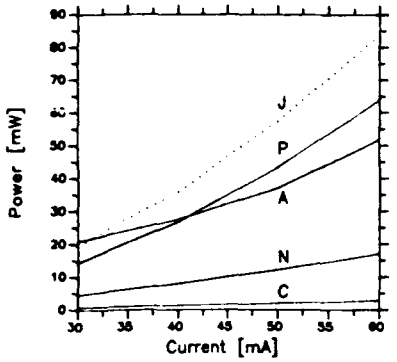

Fig. 8. Current dependence of heat generation power due to various heat sources in etched-well VC-SEL. A—heating due to nonradiative recombination and reabsorption in the p-GaAs layer containing the active region; P and N—Joule heating in P-$Al_{0.3}Ga_{0.7}As$ and N-$Al_{0.3}Ga_{0.7}As$ layers, respectively; C—Joule heating in the contact layer; J—total Joule heating (the sum of P, N, and C).

proximately quadratic dependence of Joule heating on current. The aggregate effect of Joule heating in all layers, shown as dotted line in Fig. 8, is the dominant heat source virtually over the entire current range considered. The active layer heating initially increases linearly with current, but starts to grow superlinearly at higher currents. This is a direct consequence of self-consistency requirement—the nonself-consistent solution for active layer heating remains linear with pumping current.

C. Temperature Profiles

Table III and Fig. 8 demonstrate the importance of inhomogeneous heat-source distribution and the key role of Joule heating in etched-well VC-SEL's. Neglecting any of these two aspects of thermal behavior is expected to result in considerable inaccuracies. Fig. 9 illustrates this point by comparing temperature profiles calculated in this work to the results obtained using earlier models. Neglecting Joule heating, as in [23], is bound to result in largely underestimated temperature increase (by a factor of two at 30 mA). At higher currents, where Joule heating becomes dominant, the error will be even more serious (close to a factor of three at 50 mA, not shown in Fig. 9). On the other hand, assuming homogeneous distribution of heat sources and neglecting any heat-flux spreading, as in [16], will artificially augment the temperature increase in the active region, since no allowance is made for heat transfer to surrounding layers (region II in our model). This leads to an overestimate of the active region heating at 30 mA by more than a factor of three.

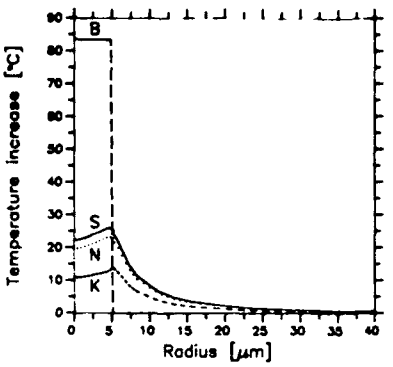

Fig. 9. Comparison of temperature profiles in the p-GaAs layer containing the active region, calculated using various thermal models of etched-well VC-SEL. S—thermal-electrical self-consistent solution; N—not self-consistent solution; B—one-dimensional model of [16]; K—model of [23] ignoring Joule heating. The total pumping current is 30 mA.

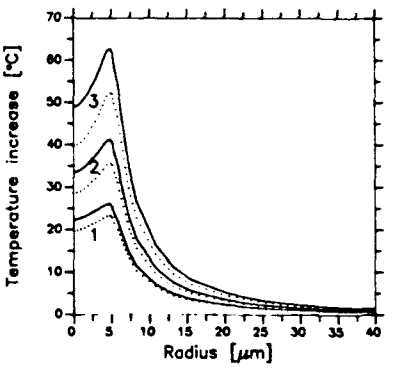

Fig. 10. Self-consistent (solid lines) and not self-consistent (dotted lines) temperature profiles in the p-GaAs layer containing the active region, for various pumping levels. Curve 1—I_T = 30 mA; curve 2—I_T = 40 mA; curve 3—I_T = 50 mA.

Fig. 10 illustrates the importance of self-consistent treatment for calculated temperature profiles. Not surprisingly, the difference between self-consistent and not self-consistent solutions increases with pumping current. Another very important feature is the temperature dip in the center of the active region. Since the refractive index increases with temperature [45], this implies that a thermal antiwaveguide is formed. The effect is enhanced at higher currents, with as much as 15°C variation for I_T = 50 mA. Since the structure contains no built-in lateral waveguide, thermal antiguiding will have significant impact on waveguiding properties of etched-well VC-SEL's. We conjecture that this effect may also play a positive role in increasing the maximum optical output power due to a wider spot size of the fundamental mode in the case of antiguiding.

We have established in Section IV-A that the doping level of the N-$Al_{0.3}Ga_{0.7}As$ layer plays a crucial role in controlling homogeneity of current density distribution in the active region. Fig. 11 illustrates consequences of varying the N-$Al_{0.3}Ga_{0.7}As$ doping for temperature profiles. Since the average current density within the active

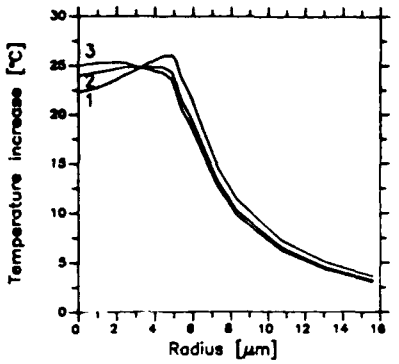

Fig. 11. Effect of varying N-$Al_{0.3}Ga_{0.7}As$ layer doping on temperature profiles in the p-GaAs layer containing the active region. Curve 1—donor concentration of 7×10^{17} cm^{-3}; curve 2—2×10^{18} cm^{-3}; curve 3—7×10^{18} cm^{-3}.

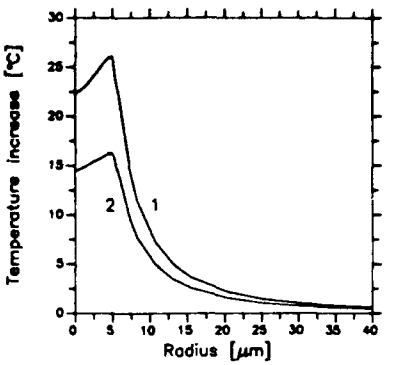

Fig. 12. Effect of varying P-$Al_{0.3}Ga_{0.7}As$ layer doping on temperature profiles in the p-GaAs layer containing the active region. Curve 1—acceptor concentration of 7×10^{17} cm^{-3}; curve 2—7×10^{18} cm^{-3}.

region changes very little [cf. Fig. 7(a)], the average temperature of the active region also remains nearly constant. However, changing the N-$Al_{0.3}Ga_{0.7}As$ doping significantly affects the actual temperature profile, thus offering the means to control the nature of thermal guiding from strong antiguiding (curve 1) through weak antiguiding (curve 2) to reversing the sign of the effect and achieving thermal focusing (curve 3). Depending on specific practical requirements for a given application, all of these effects may be of interest. The ability to engineer thermal waveguiding in etched-well VC-SEL's by rather simple technological process represents a significant advantage of these devices compared to edge emitters.

Intense heating of the active region inevitably increases the threshold current density and limits the optical output power. Apart from the active layer heating, the most important heat source is Joule heating in P-$Ala_{0.3}Ga_{0.7}As$ layer. We can therefore expect that reduction of resistivity in this layer should lead to considerable improvement in the device performance. Fig. 12 shows that it is indeed possible to reduce significantly the active region heating by increasing the doping level of P-$Al_{0.3}Ga_{0.7}As$ region. As opposed to a similar effect obtained by increasing the doping level in p-GaAs layer, this scheme does not result in reduction of the density of current flowing through the active region [cf. Fig. 7(b)]. Thus, higher doping of P-$Al_{0.3}Ga_{0.7}As$ region is the most effective way to ease the thermal problems in etched-well VC-SEL's.

D. Consequences for Two-Dimensional Integration

As a final note, we discuss the impact of thermal effects on large-scale two-dimensional integration of VC-SEL's. It can be appreciated, by examining Fig. 10, that while the temperature drops rapidly outside the active region, a long tail penetrating far away from the active element exists. If we consider a densely packed array of 10-μm-diameter emitters with 20 μm center-to-center spacing [40], thermal contributions from all 12 neighbors located within a distance of 40 μm will add to as much as 16°C at the location of the central element. This is almost as large as the temeprature increase due to the element itself, which clearly demonstrates how critical is the thermal crosstalk problem for large-scale integration.

The model presented in this paper offers a useful design tool for optimization of two-dimensional arrays. In order to avoid a costly and time-consuming process of trial and error in selecting an optimum distance between the array elements, it becomes imperative to consider thermal effects at the stage of designing the device. It is also very important to avoid using oversimplified thermal models of VC-SEL's, since they lead to gross errors in predicted thermal properties.

V. Conclusions

In spite of the severity of thermal problems in vertical-cavity surface-emitting lasers, there has been no adequate treatment of thermal properties of these devices. Previous approaches suffered from oversimplified assumptions such as one-dimensional heat flow or absence of Joule heating. In this work, a comprehensive two-dimensional thermal-electrical self-consistent model of VC-SEL's is formulated. Major heat sources are identified, and their spatial distribution is determined by analyzing current spreading in the device. Temperature profiles due to individual heat sources are calculated, and their aggregate effect is examined. Various new aspects of etched-well VC-SEL behavior are revealed. Unless careful design is undertaken, which should involve thermal analysis such as given in this work, the device may suffer from poor overlap between the optical field and gain profiles, which inevitably would increase its threshold. Novel horizons for thermal waveguide engineering are opened by the ability to control the sign and magnitude of the guiding effect simply by changing the N-$Al_{0.3}Ga_{0.7}As$ layer doping. An effective technique for reducing the extent of heating processes by increasing the P-$Al_{0.3}Ga_{0.7}As$ layer doping is suggested. It is also observed that heating problems must be considered in the design of large-scale densely packed two-dimensional arrays, where accumulation of contributions from the near and distant neighbors is expected to be a major factor limiting the array performance. We con-

clude that the present model represents an indispensable tool in the design of high-performance VC-SEL's operating CW at room temperature.

Acknowledgment

We are indebted to S. Kubica for his expert computational assistance during the course of this work.

References

[1] K. Iga, F. Koyama, and S. Kinoshita, "Surface emitting semiconductor lasers," *IEEE J. Quantum Electron.*, vol. 24, pp. 1845-1855, Sept. 1988, and the references quoted therein.

[2] J. L. Jewell, Y. H. Lee, A. Scherer, S. L. McCall, N. A. Olsson, J. P. Harbison, and L. T. Florez, "Surface-emitting microlasers for photonic switching and interchip connections," *Opt. Eng.*, vol. 29, pp. 210-214, Mar. 1990.

[3] M. Osiński, "Vertical-cavity surface-emitting semiconductor lasers for optical interconnections (invited paper)," in *Proc. 1st Int. Workshop Photon. Networks, Components, Appl.*, Montebello, P.Q., Canada, Oct. 11-13, 1990; Series in *Optics and Photonics*, vol. 2, J. Chrostowski and J. Terry, Eds. Singapore: World Scientific 1991, pp. 70-80.

[4] S. Uchiyama and K. Iga, "Two-dimensional array of GaInAsP/InP surface-emitting lasers," *Electron. Lett.*, vol. 21, pp. 162-164, Feb. 14, 1985.

[5] F. Koyama, S. Kinoshita, and K. Iga, "Room temperature cw vertical cavity surface emitting laser and high power 2-D laser array," in *Tech. Dig., CLEO '89*, Baltimore, MD, Apr. 24-28, 1989, pp. 380-381, Paper FC1.

[6] T. Sakaguchi, F. Koyama, and K. Iga, "Vertical cavity surface-emitting laser with an AlGaAs/AlAs Bragg reflector," *Electron. Lett.*, vol. 24, pp. 928-929, July 21, 1988.

[7] F. Koyama, S. Kinoshita and K. Iga, "Room-temperature continuous wave lasing characteristics of a GaAs vertical cavity surface-emitting laser," *Appl. Phys. Lett.*, vol. 55, pp. 221-222, July 17, 1989.

[8] A. Ibaraki, K. Kawashima, K. Furusawa, T. Ishikawa, T. Yamaguchi, and T. Niina, "Buried heterostructure GaAs/GaAlAs distributed Bragg reflector surface emitting laser with very low threshold (5.2 mA) under room temperature CW conditions," *Japan. J. Appl. Phys.*, vol. 28, pp. L667-L668, Apr. 1989.

[9] D. Botez, L. M. Zinkiewicz, T. J. Roth, L. J. Mawst, and G. Peterson, "Low-threshold-current-density vertical-cavity surface-emitting AlGaAs/GaAs diode lasers," *IEEE Photon. Technol. Lett.*, vol. 1, pp. 205-208, Aug. 1989.

[10] W. Hsin, G. Du, J. K. Gamelin, K. J. Malloy, S. Wang, J. R. Whinnery, Y. J. Yang, T. G. Dziura, and S. C. Wang, "Low threshold distributed Bragg reflector surface emitting laser diode with semiconductor air-bridge-supported top mirror," *Electron. Lett.*, vol. 26, pp. 307-308, Mar. 1, 1990.

[11] E. F. Schubert, L. W. Tu, R. F. Kopf, G. J. Zydzik, and D. G. Deppe, "Low-threshold vertical cavity surface-emitting lasers with metallic reflectors," *Appl. Phys. Lett.*, vol. 57, pp. 117-119, July 9, 1990.

[12] M. Shimada, T. Asaka, Y. Yamasaki, H. Iwano, M. Ogura, and S. Mukai, "Low-threshold surface-emitting laser diodes with distributed Bragg reflectors and current blocking layers," *Appl. Phys. Lett.*, vol. 57, pp. 1289-1291, Sept. 24, 1990.

[13] M. Orenstein, A. C. Von Lehmen, C. Chang-Hasnain, N. G. Stoffel, J. P. Harbison, L. T. Florez, E. Clausen, and J. E. Jewell, "Vertical-cavity surface-emitting InGaAs/GaAs lasers with planar lateral definition," *Appl. Phys. Lett.*, vol. 56, pp. 2384-2386, June 11, 1990.

[14] R. S. Geels and L. A. Coldren, "Submilliamp threshold vertical-cavity laser diodes," *Appl. Phys. Lett.*, vol. 57, pp. 1605-1607, Oct. 15, 1990.

[15] T. R. Chen, L. Eng, B. Zhao, Y. H. Zhuang, S. Sanders, H. Markoc, and A. Yariv, "Submilliamp threshold InGaAs/GaAs strained layer quantum-well laser," *IEEE J. Quantum Electron.*, vol. 26, pp. 1183-1190, July 1990.

[16] R. Baets, "Considerations on geometry design of surface-emitting laser diodes," *IEE Proc. Pt. J (Optoelectron.)*, vol. 135, pp. 233-241, June 1988.

[17] W. Nakwaski, "Correspondence: Considerations on geometry design of surface-emitting laser diodes," *IEE Proc. Pt. J. (Optoelectron.)*, vol. 137, pp. 129-131, Apr. 1990.

[18] K. Tai, R. J. Fischer, C. W. Seabury, N. A. Olsson, T.-C. D. Huo, Y. Ota, and A. Y. Cho, "Room-temperature continuous-wave vertical-cavity surface-emitting GaAs injection lasers," *Appl. Phys. Lett.*, vol. 55, pp. 2473-2475, Dec. 11, 1989.

[19] E. Duda, J.-C. Carballes, and J. Apruzzese, "Thermal resistance and temperature distribution in double-heterostructure lasers: Calculations and experimental results," *IEEE J. Quantum Electron.*, vol. QE-15, pp. 812-817, Aug. 1979.

[20] M. Yano, H. Imai, K. Hori, and M. Takusagawa, "High temperature characteristics of stripe-geometry InGaAsP/InP double-heterostructure lasers," *IEEE J. Quantum Electron.*, vol. QE-17, pp. 619-626, May 1981.

[21] M. Ito and T. Kimura, "Stationary and transient thermal properties of semiconductor laser diodes," *IEEE J. Quantum Electron.*, vol. QE-17, pp. 787-795, May 1981.

[22] J. S. Manning, "Thermal impedance of diode lasers: Comparison of experimental methods and a theoretical model," *J. Appl. Phys.*, vol. 52, pp. 3179-3184, May 1981.

[23] S. Kinoshita, F. Koyama, and K. Iga, "Investigation of the CW operation at room temperature for GaAlAs/GaAs surface emitting laser," in *Proc. Tech. Group Meet., IECE Japan*, Mar. 16, 1987, pp. 23-30, Paper OQE86-188.

[24] G. R. Hadley, J. P. Hohimer, and A. Owyoung, "Comprehensive modelling of diode arrays and broad-area devices with applications to lateral index tailoring," *IEEE J. Quantum Electron.*, vol. 24, pp. 2138-2152, Nov. 1988.

[25] C. H. Henry, R. A. Logan, and F. R. Merritt, "The effect of surface recombination on current in $Al_xGa_{1-x}As$ heterojunctions," *J. Appl. Phys.*, vol. 49, pp. 3530-3542, June 1978.

[26] M. Bugajski and A. M. Kontkiewicz, "Steady-state distributions of current and junction potential in high radiance LEDs for optical communication systems," *Electron Technol.*, vol. 13, no. 4, pp. 63-79, 1982.

[27] T. Kobayashi and Y. Furukawa, "Temperature distributions in the GaAs-AlGaAs double-heterostructure laser below and above the threshold current," *Japan. J. Appl. Phys.*, vol. 14, pp. 1981-1986, Dec. 1975.

[28] W. Nakwaski, "Spontaneous radiation transfer in heterojunction laser diodes," *Sov. J. Quantum Electron.*, vol. 9, pp. 1544-1546, Dec. 1979.

[29] R. Papannareddy, W. Ferguson, and J. K. Butler, "A generalized thermal model for stripe-geometry injection lasers," *J. Appl. Phys.*, vol. 62, pp. 3565-3569, Nov. 1, 1987.

[30] W. Nakwaski, "Thermal properties of the Burrus-type light-emitting diode: Part I—The model," *IEEE Trans. Electron Devices*, vol. ED-33, pp. 889-899, July 1986.

[31] W. Nakwaski and A. M. Kontkiewicz, "Thermal resistance of light-emitting diodes," *IEEE Trans. Electron Devices*, vol. ED-32, pp. 2282-2291, Nov. 1985.

[32] J. C. Carslaw and J. C. Jaeger, *Conduction of Heat in Solids*. Clarendon, England: Clarendon, 1986, p. 216.

[33] S. Kinoshita, T. Sakaguchi, T. Odagawa, and K. Iga, "GaAlAs/GaAs surface emitting laser with high reflective TiO_2/SiO_2 multilayer Bragg reflector," *Japan. J. Appl. Phys.*, vol. 26, pp. 410-415, Mar. 1987.

[34] F. Koyama, H. Uenohara, T. Sakaguchi, and K. Iga, "GaAlAs/GaAs MOCVD growth for surface emitting lasers," *Japan. J. Appl. Phys.*, vol. 26, pp. 1077-1081, July 1987.

[35] S. M. Sze and J. C. Irvin, "Resistivity, mobility and impurity levels in GaAs, Ge, and Si at 300° K," *Solid-State Electron.*, vol. 11, pp. 599-602, June 1968.

[36] G. B. Stringfellow, "Electron mobility in $Al_xGa_{1-x}As$," *J. Appl. Phys.*, vol. 50, pp. 4178-4183, June 1979.

[37] K. Tai, L. Yang, Y. H. Wang, J. D. Wynn, and A. Y. Cho, "Drastic reduction of series resistance in doped semiconductor distributed Bragg reflectors for surface-emitting lasers," *Appl. Phys. Lett.*, vol. 56, pp. 2496-2498, June 18, 1990.

[38] Y. S. Touloukian, R. W. Powell, C. Y. Ho, and P. G. Klemens, *Thermophysical Properties of Matter, Vol. 2: Thermal Conductivity, Nonmetallic Solids*. New York: IFI/Plenum, 1970, Tables 32R and 36P.

[39] D. E. Gray, Ed., *American Institute of Physics Handbook*. New York: McGraw-Hill, 1972, Table 4g-8.

[40] F. Koyama, K. Tomomatsu, and K. Iga, "GaAs surface emitting lasers with circular buried heterostructure grown by metalorganic chemical vapor deposition and two-dimensional laser array," *Appl. Phys. Lett.*, vol. 52, pp. 528-529, Feb. 15, 1988.

[41] S. Adachi, "Lattice thermal resistivity of III-V compound alloys," *J. Appl. Phys.*, vol. 54, pp. 1844-1848, Apr. 1983.

[42] A. Amith, I. Kudman, and E. F. Steigmeier, "Electron and phonon scattering in GaAs at high temperatures," *Phys. Rev.*, vol. 138, pp. A1270-A1276, May 17, 1965.
[43] P. Garel-Jones and J. C. Dyment, "Calculations of the continuous-wave lasing range and light-output power for double-heterostructure lasers," *IEEE J. Quantum Electron.*, vol. QE-11, pp. 408-413, July 1975.
[44] N. K. Dutta, "Analysis of current spreading, carrier diffusion, and transverse mode guiding in surface emitting lasers," *J. Appl. Phys.*, vol. 68, pp. 1961-1963, Sept. 1, 1990.
[45] J. S. Blakemore, "Semiconducting and other major properties of gallium arsenide," *J. Appl. Phys.*, vol. 53, pp. R123-R181, Oct. 1982.

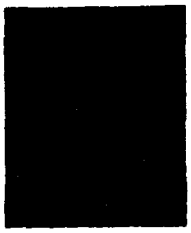

Włodzimierz Nakwaski was born in Łódź, Poland, on April 13, 1947. He received the M.Sc. degree in electrical engineering from the Technical University of Łódź in 1971, the M.Sc. degree in physics from Łódź University in 1973, and the Ph.D. (cum laude) and D.Sc. degrees in electrical engineering from the Institute of Electron Technology, Warsaw, Poland, in 1976 and 1985.

In 1974 he joined the Institute of Electron Technology, Warsaw, where he was engaged in theoretical and experimental investigations of diode lasers and LED's. Since 1976 he has been with the Institute of Physics and the Department of Technical Physics and Applied Mathematics, Technical University of Łódź, where he is now Associate Professor. From August 1981 until December 1981 he was a Postdoctoral Research Associate at the Technical University of Denmark, Lyngby. Since 1974 his research efforts have been focused on thermal properties of optoelectronic devices. In 1990 he was the recipient of an IREX grant for international exchange of scholars with the United States. Since September 1990 he has been a Visiting Senior Research Scientist with the Center for High Technology Materials, University of New Mexico, Albuquerque. His present research interests include theoretical investigations of thermal behavior of diode lasers and LED's, catastrophic degradation, and thermal properties of III-V compounds. He has authored or coauthored over 100 technical papers and two books: *Semiconductor Lasers* (Polish Scientific Publishers (in Polish), 1985) and *Physics of Semiconductor Lasers* (North-Holland/Elsevier).

Dr. Nakwaski is a member of the International Society for Optical Engineering (SPIE).

Marek Osiński (SM'86) was born in Wrocław, Poland, on May 28, 1948. He received the M.Sc. degree in theoretical physics from Warsaw University, Warsaw, Poland, in 1971 and the Ph.D. degree in physical sciences from the Institute of Physics of the Polish Academy of Sciences (PASc), Warsaw, in 1979.

In 1971 he joined the Institute of Physics of PASc, where he was engaged in investigations of waveguiding properties and modal characteristics of semiconductor lasers. From November 1980 until June 1984 he was a Visiting Research Fellow at Southampton University, England, where he conducted research on long-wavelength injection laser properties relevant to optical fiber communications. He also investigated optical properties of III-V compounds and heterostructures, including quantum-well devices. From July 1984 until August 1985 he was a British Telecom Senior Research Associate in Coherent Optical Communication at Cambridge University, England, where he was involved in studying picosecond modulation, gain-switched spectra, external-cavity coupling, and injection locking of diode lasers. Since 1985 he has been an Associate Professor with the Center for High Technology Materials, University of New Mexico, Albuquerque, where he is also a Faculty member in the Department of Electrical and Computer Engineering and the Department of Physics and Astronomy. From July 1988 to August 1989 he held the NTT Endowed Chair in Telecommunications as a Visiting Professor at the Research Center for Advanced Science and Technology, University of Tokyo, Tokyo, Japan. His main current research interests include high-power semiconductor laser arrays, surface-emitting lasers, thermal properties of semiconductor lasers, spatially filtered external cavity coupling and side-mode injection locking, optoelectronic structures with low dimensionality, and material properties of AlGaAs and InGaAsP alloys. He has authored or coauthored over 125 technical papers.

Dr. Osiński is a member of the IEEE Lasers and Electro-Optics Society, the Optical Society of America, the International Society for Optical Engineering (SPIE), the European Physical Society, Sigma Xi, and the New Mexico Section of Materials Research Society. He is listed in *American Men and Women of Science*.

In print, SPIE Proc. Vol. 1418 - Laser Diode Techn. & Appl. III, (D. Renner, Ed.), Los Angeles, CA, 20-25.01.1991

NOVEL DISTRIBUTED-FEEDBACK STRUCTURE FOR SURFACE-EMITTING SEMICONDUCTOR LASERS

Mohammad Mahbobzadeh* and Marek Osiński**

Center for High Technology Materials, University of New Mexico, Albuquerque, New Mexico 87131-6081

ABSTRACT

A novel distributed feedback structure for wavelength-resonant surface-emitting semiconductor lasers is proposed and demonstrated. Compared to earlier resonant-periodic-gain devices, the total thickness of the new structure can be considerably smaller while retaining the characteristic features of the resonant-periodic-gain active medium. Room-temperature cw and pulsed operation of first distributed-feedback resonant-periodic-gain AlGaAs/GaAs/AlAs laser is reported.

1. INTRODUCTION

Surface-emitting semiconductor lasers are attracting considerable attention due to a wide range of their potential applications. There have been several approaches (vertical resonators, second-order grating coupling, and inclined mirrors) to achieve emission of the laser beam through the top surface. Among these, vertical-cavity surface-emitting lasers (*VC-SELs*)[1,2] offer distinct advantages of planar geometry, stable single-longitudinal-mode oscillation, and low-divergence circular output beam. Small-area low-threshold-current lasers can be used in optical computing and can be integrated with other optoelectronic devices to form part of monolithic optoelectronic integrated circuits and optical interconnects. Their low beam divergence simplifies the optics requirements and facilitates coupling into optical fibers. VC-SELs can also be easily arranged in one- or two-dimensional arrays to form high-power sources with possible applications in free-space optical communications and in solid-state laser pumping.

Conventional VC-SELs suffer from low external efficiencies and consequently low output powers. The primary reason for their poor performance lies in the competition between the desirable vertical emission and parasitic amplification of radiation emitted spontaneously in the directions parallel to the substrate plane. In order to suppress the amplified spontaneous emission (ASE) in the transverse directions and reduce the lasing threshold, a resonant-periodic-gain (RPG) structure has been proposed[3-6]. The RPG design takes advantage of the vertical geometry of VC-SELs by aligning quantum-well active regions, spaced at half the wavelength of a selected optical transition, with the maxima of the longitudinal mode pattern at the design wavelength. This enhances the gain along the vertical direction at the design wavelength and discriminates against the ASE parallel to the wafer surface. In addition, more efficient pumping is achieved and excitation of regions adjacent to the nulls of the standing wave is eliminated. In order to achieve low threshold, the RPG active region is normally sandwiched between two multilayer high reflectors (MHR), thus forming a distributed-Bragg-reflector (DBR) cavity with

---

* Also with the Department of Electrical and Computer Engineering, University of New Mexico.

** Also with the Department of Physics and Astronomy, University of New Mexico.

relatively large total thickness.

In this paper, we present a new distributed-feedback (DFB) structure for RPG lasers which eliminates the need for end reflectors by interlacing the quarter-wave multilayer high reflectors with the gain medium. This reduces considerably the total thickness of the device, while retaining the characteristic features of the RPG active medium. We report on the first implementation of the new concept, using an optically pumped MO-CVD grown wafer. Both cw and pulsed operation is investigated. Preliminary results indicate that the new structure has indeed potential for very high output power.

2. CONCEPT OF DISTRIBUTED-FEEDBACK RESONANT-PERIODIC-GAIN MEDIUM

The length of DBR-type structures is inherently greater than that of otherwise equivalent DFB devices because the amplifying and feedback sections overlap in the latter structures. For VC-SELs, the device length is of primary concern, since apart from issues of technological complexity and cost it also affects the ability to pump the device uniformly. To reduce the DBR-RPG device length, we have proposed[7] that the RPG medium be converted into a DFB section by replacing the half-wave spacers with alternating quarter-wave layers which would provide reflectivity required for feedback. The resultant DFB-RPG structure is schematically illustrated in Figs. 1 and 2. A vertical resonator with highly reflective mirrors is created by a stack of alternating high- and low-refractive-index quarter-wave layers that form a DFB medium (layers C and D of Fig. 1, with refractive indices μ_C, μ_D). Within the DFB region, an RPG active medium is interspersed, represented in Fig. 1 by thick lines A. Each element of the RPG active medium can consist of a single quantum well or a group of coupled quantum wells positioned in such a way that they coincide with the antinodes of the standing wave at the designed wavelength of operation. This wavelength corresponds to a particular optical transition in the quantum well. The elements of the embedding DFB medium form spacers between active regions. One of the spacers, composed entirely of the high-index material B, serves as a phase shifter to satisfy the roundtrip phase matching condition.

In the following, we will describe particular design that was used to grow the first DFB-RPG AlGaAs/GaAs/AlAs wafer and report on initial results of cw and pulsed optical pumping of that prototype device.

3. PROTOTYPE DISTRIBUTED-FEEDBACK RESONANT-PERIODIC-GAIN LASER STRUCTURE

A prototype AlGaAs/GaAs/AlAs DFB-RPG VC-SEL sample was designed to operate at $n = 1$ subband transition in the quantum well. The active region consists of a stack of 10-nm thick GaAs single quantum wells separated by half-wave passive spacers. Except for a phase shifter in the central part of the structure, every spacer comprises two layers of AlAs (63.4-nm thick) and $Al_{0.15}Ga_{0.85}As$ (54.3 nm), each having an optical thickness of approximately a quarter of the design wavelength $\lambda_r = 840.4$ nm. The refractive indices for GaAs, $Al_{0.15}Ga_{0.85}As$, and AlAs were taken as 3.60, 3.50, and 3.00, respectively.[8] The lower and upper portions of the structure are separated by an $Al_{0.15}Ga_{0.85}As$ phase shifter with optical thickness of approximately $\lambda_r/2$. The whole structure contains 42.5 periods, of which 24 periods, counting from the center of the phase shifter, are at the bottom (*i.e.*, at the GaAs substrate side) and 18.5 periods are at the top. The output light is collected through the top surface. Since no quantum well is adjacent to the very first quarter-wave layer located at the top surface, the Al content in this layer is increased to 20% in order to avoid undesirable absorption of the pump light. The thickness of that layer is 59.9 nm, corresponding to the refractive index of 3.47.[8]

The total thickness of the structure described above, including the quantum-well layers, is approximately 5.42 μm. For the sake of comparison, a DBR-RPG laser with the same cumulative thickness of the active medium and the same reflectivities of multilayer reflectors would be almost two times thicker (10.55 μm) than the DFB-RPG structure.

Figs. 3(a) and 3(b) illustrate cavity reflectivity and gain spectra calculated for the DFB-RPG structure described above and for an equivalent RPG device with Bragg reflectors. The method of calculation follows a standard approach for periodic stratified media[9]. The transfer matrix for the structure is simplified by noting that products of identical unimodular matrices can be calculated analytically. Calculated reflectivities of the lower and upper reflectors are 99.76% and 99.56%, respectively. The most remarkable difference between the two structures is the absence of any side modes within the high-reflectivity band of the DFB-RPG laser. This is a direct consequence of shorter cavity length. Strong enhancement of gain at the resonance illustrates excellent wavelength selectivity of our structure.

In the process of designing the DFB-RPG structure, we used the reflectivity calculations to check for the wavelength of resonant mode. When the total optical thickness of a single period, consisting of a quantum well and an AlAs/$Al_{0.15}Ga_{0.85}As$ "half-wave" spacer, was chosen to be exactly equal to half of the design wavelength taken as 840.4 nm, the calculated resonant wavelength was longer (~848 nm) than the design wavelength. We attribute this shift of resonant wavelength to a phase-disturbing effect of quantum well layers. In order to correct for this shift, we have slightly reduced thicknesses of all spacer layers, thus bringing the resonance back to 840.4 nm.

4. EXPERIMENTAL RESULTS

The MOCVD-grown prototype structure described in previous section was optically pumped through the top mirror. The as-grown wafer was mounted in a holder, without any provision for heat-sinking. In order to enhance pumping efficiency, pumping wavelengths of 735-740 nm was selected. The corresponding photon energies of 1.68-1.69 eV are larger than the bandgap of $Al_{0.15}Ga_{0.85}As$ spacers (1.63 eV)[10] but smaller than the bandgap of the cap $Al_{0.2}Ga_{0.8}As$ layer (1.70 eV).[10] Hence, the pumping light was absorbed in $Al_{0.15}Ga_{0.85}As$ spacers, generating free carriers which subsequently could fall into quantum well GaAs active regions. This indirect pumping combined with absorption in quantum wells results in an improved pumping efficiency.

Since no heat sink was used, we anticipated that cw output power would be seriously limited by thermal effects. Therefore, with the aim of determining the potential of DFB-RPG lasers for high-power operation, we performed both pulsed and cw input/output measurements.

The experimental arrangement used for measurements of the pulsed input/output characteristics is shown schematically in Fig. 4. For pumping the DFB-RPG structure through the top surface, we used a dye laser (Quanta-Ray PDL-1, 230 μJ single-pulse energy), pumped by a Nd:YAG laser (Quanta-Ray DCR-2). The dye laser emitted 7 ns pulses at 10 Hz repetition rate, and was tuned to 735 nm wavelength. The pump beam power could be altered gradually by adjusting a variable neutral-density (ND) attenuator. A high-transmission, low-reflection (90/10) beam splitter BS allowed a direct measurement of the input power by reading the transmitted part of the pump power and multiplying it by a calibration factor that converted the transmitted power into the input power. A calibrated Gentec photodetector was used for this purpose. A calibrated dichroic beam splitter DBS was used to redirect the pump beam on its path towards the sample and to separate the reflected portion of the pump beam from the DFB-RPG output. Additional calibrated ND filter was inserted between the beam splitters BS and DBS to further attenuate the pump beam. A 10× microscope objective served a dual purpose of focusing the

pump beam and collimating the output. The DFB-RPG output power was measured using a Si photodetector calibrated to give the single-pulse output energy. Residual reflected pump beam was eliminated by an interference filter placed between the beam splitter DBS and the Si detector.

The experimental setup for cw measurements was essentially similar to that shown in Fig. 4. A dye laser (Coherent CR-599, 200 mW) operating at 740-nm wavelength, pumped by cw argon-ion laser (Spectra Physics Series 2000), was used as a pump source. The beam splitter BS was replaced by another beam splitter having low transmission (10%) and high reflection (90%), and no detector was placed behind BS. Calibrated power meters were employed to measure pumping and output power just prior to microscope objective and just after the interference filter, respectively. Spectral measurements were performed by coupling the DFB-RPG laser output into a high-resolution spectrometer by means of an optical fiber placed in a position of Si detector in Fig. 4. Appropriate interference filters were used between the beam splitter DBS and the fiber to select either pump signal or DFB-RPG output.

Fig. 5 shows a typical input/output characteristic for room-temperature cw pumping. The pump power values have been corrected for measured reflection from the surface (~32%) and calculated transmission (8%) through the DFB-RPG section. The lasing threshold for 10-μm spot size is ~60 mW, with top-surface output power efficiency of 9.3%, and differential quantum efficiency exceeding 80%. The maximum output of 6.7 mW is obviously limited by heating effects.

The output spectra centered at ~878 nm were rather broad (0.8 nm) with a complex structure indicating multiple transverse mode operation. Further work on improving the design with the goal of reducing the spectral width is in progress.

An input/output characteristic under pulsed pumping conditions is shown in Fig. 6. The output power of 8.5 W over 7 ns pulsewidth with power conversion efficiency of 10.5% is obtained. To our best knowledge, this is the highest peak power ever reported for VC-SEL devices. These data are preliminary and at this time a reliable estimate of maximum power density cannot be given. This is due to the fact that the beam was defocused slightly in order to maximize the output power and therefore the spot size is not exactly known. Further experiments are underway to determine the actual spot size. However, the several orders of magnitude difference between the pulsed and cw maximum output power density is a clear indication that easing the heating problems by employing efficient heat sinking should lead to significantly higher cw output power.

5. CONCLUSIONS

A novel DFB-RPG structure for vertical-cavity surface-emitting lasers has been proposed and demonstrated. Compared to recently developed DBR-RPG structures, a reduction in the total thickness of the device by almost a factor of two is achieved by eliminating the end reflectors and by interlacing the quarter-wave multilayer high reflectors with the RPG medium. The DFB-RPG devices offer the advantages of considerably simpler fabrication process, improved wavelength selectivity, and strong discrimination against excitation of secondary longitudinal modes. Preliminary data obtained on optically pumped bare wafer sample without any heat sink indicate that very high output power should be possible. 6.7 mW cw and 8.5 W pulsed output power was measured.

6. ACKNOWLEDGMENTS

This work was partially supported by the US Air Force Office of Scientific Research and Defense Advanced Research Projects Agency. The authors are grateful to Dr. C. F. Schaus for growing the prototype DFB-RPG sample, to Miss E. Gandjbakhch for assistance in performing optical pumping experiments, and to Drs. S. R. J. Brueck and A. Mukherjee for numerous helpful discussions.

7. REFERENCES

1. M. Osiński, "Vertical-Cavity Surface-Emitting Semiconductor Lasers: Present Status and Future Prospects", this volume.

2. M. Ogura, "Progress of Surface-Emitting Lasers in Japan", this volume.

3. R. Geels, R. H. Yan, J. W. Scott, S. W. Corzine, R. J. Simes, and L. A. Coldren, "Analysis and Design of a Novel Parallel-Driven MQW-DBR Surface-Emitting Diode Laser", Techn. Digest, CLEO '88 Conf. on Lasers and Electro-Optics, Anaheim, California, 25-29 April 1988, Paper WM1, pp. 206-207.

4. M. Y. A. Raja, S. R. J. Brueck, M. Osiński, C. F. Schaus, J. G. McInerney, T. M. Brennan, and B. E. Hammons, "Wavelength-Resonant Enhanced Gain/Absorption Structure for Opto-electronic Devices", in Post-Deadline Papers, XVI Int. Conf. on Quantum Electron. IQEC'88, Tokyo, Japan, 18-21 July 1988, Paper PD-23, pp. 52-53.

5. M. Y. A. Raja, S. R. J. Brueck, M. Osiński, C. F. Schaus, J. G. McInerney, T. M. Brennan, and B. E. Hammons, "Resonant Periodic Gain Surface-Emitting Semiconductor Lasers", *IEEE J. Quantum Electron.*, vol. 25, pp. 1500-1512, June 1989.

6. S. W. Corzine, R. S. Geels, J. W. Scott, R.-H. Yan, and L. A. Coldren, "Design of Fabry-Perot Surface-Emitting Lasers with a Periodic Gain Structure" *IEEE J. Quantum Electron.*, vol. 25, pp. 1513-1524, June 1989.

7. M. Mahbobzadeh and M. Osiński, "Novel Distributed-Feedback Resonant-Periodic-Gain Structure for Vertical-Cavity Surface-Emitting Semiconductor Lasers", *Electron. Lett.*, vol. 26, pp. 1716-1718, 27 Sept. 1990.

8. J.-P. Weber, "Propagation of Light in Periodic Structures: Application to Surface-Emitting Laser Diode", Ph.D. Dissertation, University of California at Berkeley, June 1990, Appendix A, pp. 227-246.

9. M. Born and E. Wolf, Principles of Optics, 6th Edition, Pergamon Press, Oxford 1980, Ch. 1.6, pp. 51-70.

10. C. Bosio, J. L. Staehli, M. Guzzi, G. Burri, and R. A. Logan, "Direct-energy-gap dependence on Al concentration in $Al_xGa_{1-x}As$", *Phys. Rev. B*, vol. 38, pp. 3263-3266, 15 Aug. 1988.

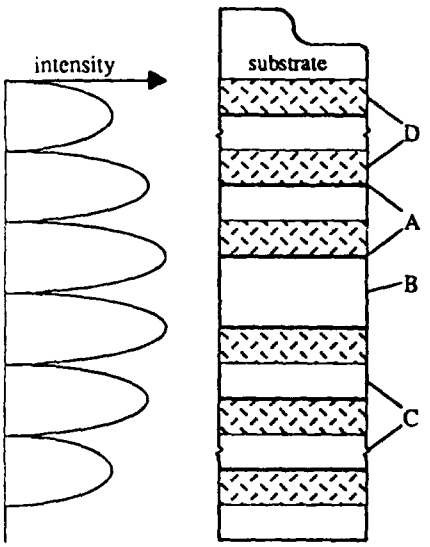

Fig. 1. A schematic illustration of the DFB-RPG structure and a corresponding intensity distribution of resonant mode. Thick lines (A) represent quantum-well active layers, unshaded region (B) - half-wave phase shifter, unshaded regions (C) - high-index quarter-wave spacers, shaded regions (D) - low-index quarter-wave spacers.

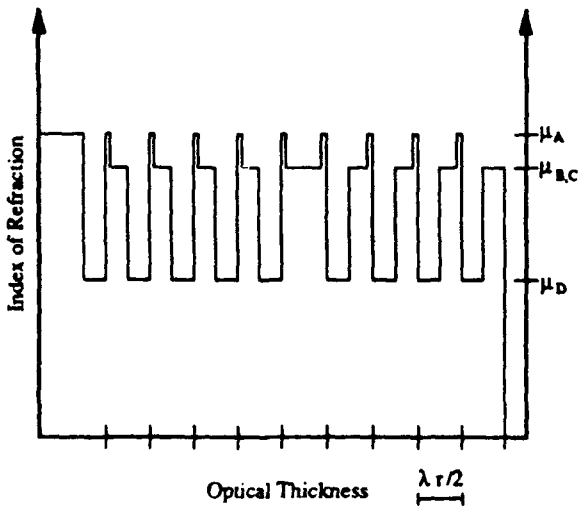

Fig. 2. Refractive index profile of the DFB-RPG structure with layer designation (A,B,C,D) the same as in Fig. 1. The number of periods is reduced to simplify graphical illustration.

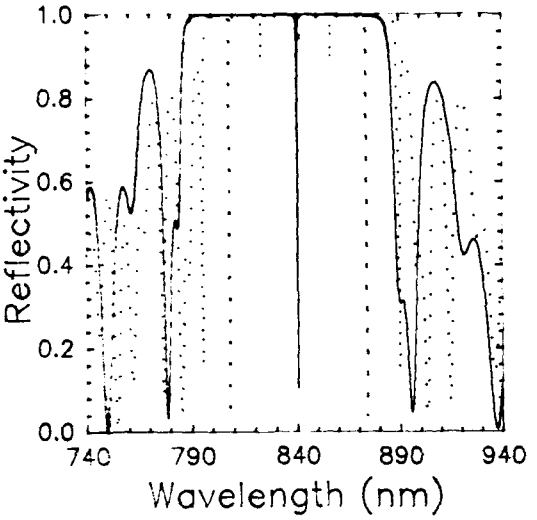

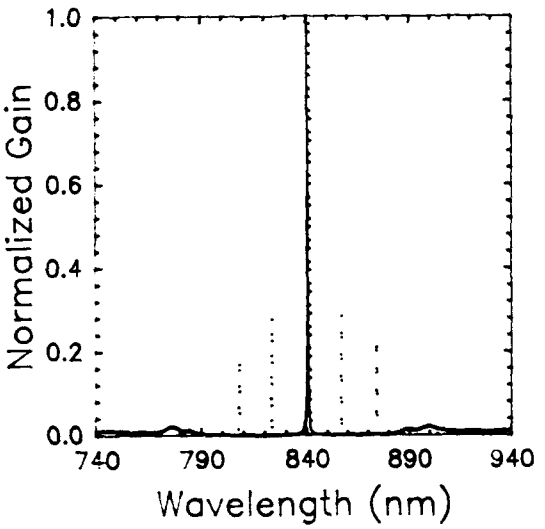

Fig. 3. Calculated reflectivity and gain spectra for a AlGaAs/GaAs/AlAs DFB-RPG VC-SEL (broken lines) and an equivalent DBR-RPG device with the same active medium thickness and MHR reflectivities (dotted lines).

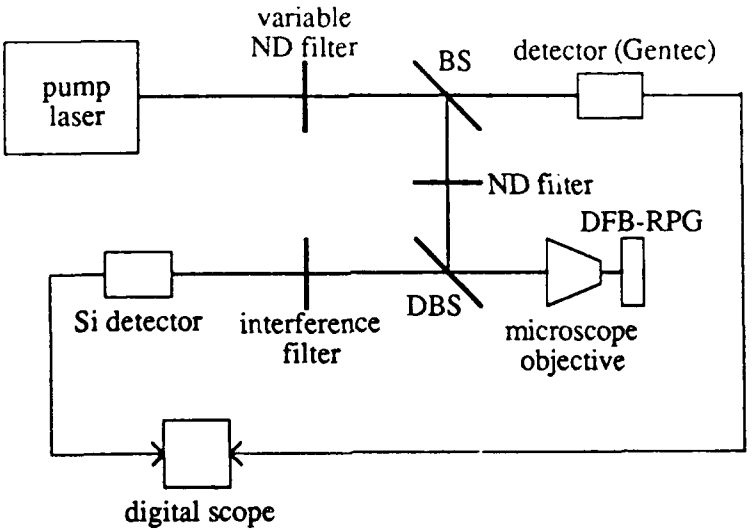

Fig. 4. Experimental setup for measurements of input/output characteristics of optically pumped VC-SELs.

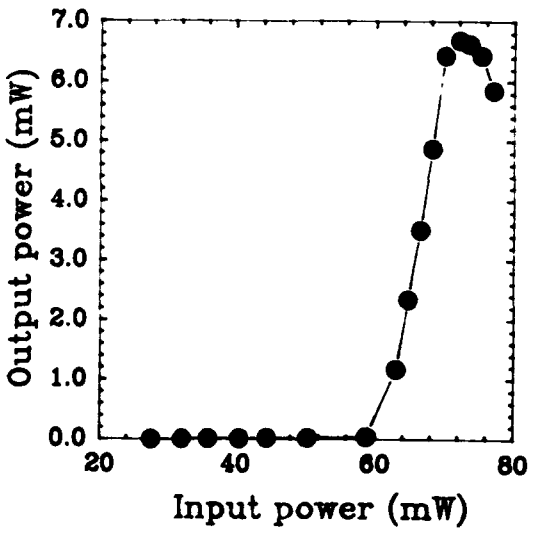

Fig. 5. Typical input/output characteristic for room-temperature cw pumping of DFB-RPG sample.

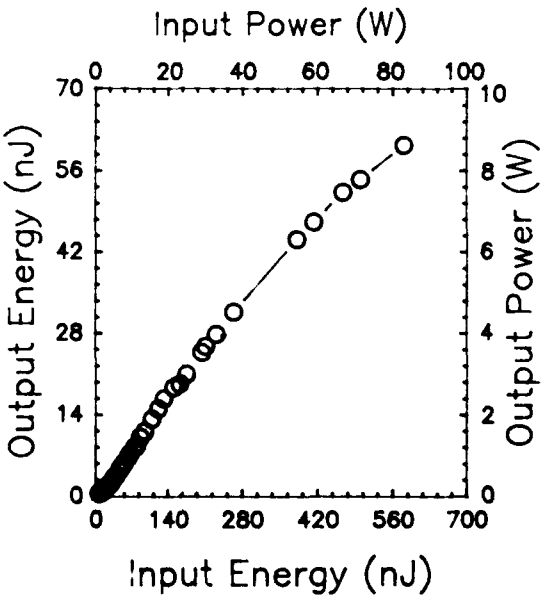

Fig. 6. Input/output characteristic for room-temperature pulsed operation of DFB-RPG laser.